TECHNISCHE UNIVERSITÄT WIEN
Vienna University of Technology

Diplomarbeit

# Adsorption of simple molecules on $TiO_2$ anatase (101) – $H_2O$, H, $CO_2$

Ausgeführt am Institut für Angewandte Physik der Technischen Universität Wien

Unter der Anleitung von
Ao.Univ.Prof. Dipl.-Ing. Dr.techn. Michael Schmid
Projektass. Martin Setvin, PhD
Univ.Prof. Dipl.-Ing. Dr.techn. Ulrike Diebold

durch
Benjamin Daniel
Mat. Nr.: 0626320
Guglgasse 8/4/8/43
1110 Wien

## *Abstract*

$TiO_2$ is a material commonly used in photocatalysis. It is mostly utilized in a powder form, which primarily consists of the metastable anatase polymorph. Contrary to the stable rutile form, anatase has not been under systematic experimental investigation as a single crystal. In this work, adsorption of simple molecules on the anatase (101) surface was studied by means of Scanning Tunneling Microscopy (STM). STM images of hydrogen, water and $CO_2$ have been obtained. Comparison to published DFT calculations allows determining adsorption configurations of these species.

The temperature-dependent behavior of these adsorbates was investigated: for H the lowest temperature where diffusion is found is 250 K. Experimental results indicate hydrogen migration into the subsurface above 350 K, preferably to defect sites. Water shows surface diffusion above 210 K and desorbs at 290 K. It was found that coadsorption of water with $O_2$ and annealing results in formation of terminal hydroxyl groups, which are stable above room temperature. $CO_2$ shows no thermally induced diffusion up to 48 K.

Interactions of the adsorbates with the STM tip were studied. H becomes mobile when scanned at high sample bias (> +2.5 V), and can be picked up by the tip. It is possible to drop H atoms back onto the surface by using a negative sample bias. $CO_2$ shows similar movement and desorption at high bias; movement also occurs at low bias (< 1 V). For water, tip-induced movement is very rare; high bias converts $H_2O$ into OH and bridging oxygen dimers.

## *Kurzfassung*

Titandioxid ist ein häufig in der Photokatalyse verwendetes Material, welches für gewöhnlich in Form eines Pulvers eingesetzt wird. Diese besteht zum Großteil aus der metastabilen $TiO_2$-Anatas-Phase. Im Gegensatz zur stabilen Rutil-Phase wurde Anatas lange nicht als Einkristall experimentell untersucht. In dieser Arbeit wurde Rastertunnelmikroskopie (STM) eingesetzt, um die Adsorption einfacher Moleküle auf der Anatas(101)-Oberfläche zu untersuchen. Vergleiche von bereits veröffentlichten DFT-Rechnungen mit STM-Bildern von adsorbiertem Wasserstoff, Wasser und $CO_2$ erlaubten die Bestimmung der Adsorptionskonfigurationen.

Das temperaturabhängige Verhalten dieser Adsorbate wurde untersucht. Die Oberflächendiffusion von Wasserstoff beginnt bei 250 K, ab 350 K wurden insbesondere an Defekten Hinweise auf Migration von H unter die Oberfläche gefunden. Die Diffusion von Wasser beginnt bei 210 K, über 290 K desorbiert es von der Oberfläche. Bei gleichzeitiger Adsorption von Wasser und $O_2$ und Erwärmung auf Raumtemperatur wurden terminale Hydroxylgruppen gefunden, welche auch bei höheren Temperaturen stabil waren.

Die Beeinflussung der Adsorbate durch die STM-Spitze wurde untersucht. Bei hoher Probenspannung (> +2.5 V) ist Wasserstoff beweglich und kann von der Spitze aufgenommen werden. Aufgenommene Atome können durch eine negative Probenspannung wieder auf die Probe transferiert werden. $CO_2$ zeigt ähnliche Beweglichkeit und auch Desorption bei hoher Probenspannung, bei niedrigen Spannungen (< 1 V) ist es ebenfalls beweglich. Bewegung durch Interaktion mit der Spitze ist bei Wasser sehr selten; hohe Spannung wandelt $H_2O$ in OH und sogenannte „bridging oxygen dimers“ um.

# Table of contents

# 1 Introduction / interest in $TiO_2$

$TiO_2$ is a commonly used material with many applications, such as a white pigment in paints and cosmetic products, optical and protective coating or biocompatibility of bone implants [1, 2].

Several other potential applications are currently hot topics in surface science:

- Uses as a photocatalyst [3, 4] (80% of heterogeneous photochemistry papers involve $TiO_2$ based materials [5])
- Dye sensitized solar cell [6-8]
- Water splitting in UV light [9-11]
- Gas sensor [12, 13]
- Memristor [14-16]

Most of the applications use nanocrystalline powders such as Degussa P25 [17]. However, single crystals are necessary for fundamental research under well-defined conditions

## 1.1 Polymorphs of $TiO_2$

Most of surface science research on $TiO_2$ was done on rutile, which is the most common and the most stable polymorph of $TiO_2$. It is easy to grow as single crystals of high purity. Other polymorphs, such as anatase or brookite, were ignored for a long time, as good single crystalline samples are hard to come by. Lately the $TiO_2$ anatase phase has received increasing attention since it commonly appears in $TiO_2$ nanopowders such as Degussa P25 (a mixture of nanoscale anatase and rutile), which is used as a 'benchmark' in photocatalysis.

### 1.1.1 Rutile

Rutile is the thermodynamically most stable polymorph of $TiO_2$. It is a transparent semiconductor that turns yellow when heated above 200°C and black when it is sufficiently reduced. The commonly used (110) surface is the most stable of all $TiO_2$ surfaces and usually exhibits around 5-15% surface oxygen vacancies when prepared under UHV conditions [1, 18-20].

| | Rutile | Anatase | Ref |
|---|---|---|---|
| Space group | $P4_2/mnm$ | $I4_1/amd$ | [21] |
| Bandgap | 3 eV (direct) | 3.2 eV (indirect) | [5] |
| Density | 4.25 g/cm$^3$ | 3.894 g/cm$^3$ | [21] |
| Unit cell dimensions | a = 0.4593 nm<br>c = 0.2959 nm | a = 0.3785 nm<br>c = 0.9512 nm | [22] |
| Surface energy | 0.35 J/m$^2$ (110) | 0.49 J/m$^2$ (101) | [18] |

Table 1: Properties of anatase and rutile

### 1.1.2 Anatase

Anatase is a metastable polymorph of $TiO_2$ that is irreversibly transformed into rutile at temperatures between 600 and 700°C. This transformation is highly dependent on many parameters such as atmosphere, homogeneity, impurities, and crystallite size [21].

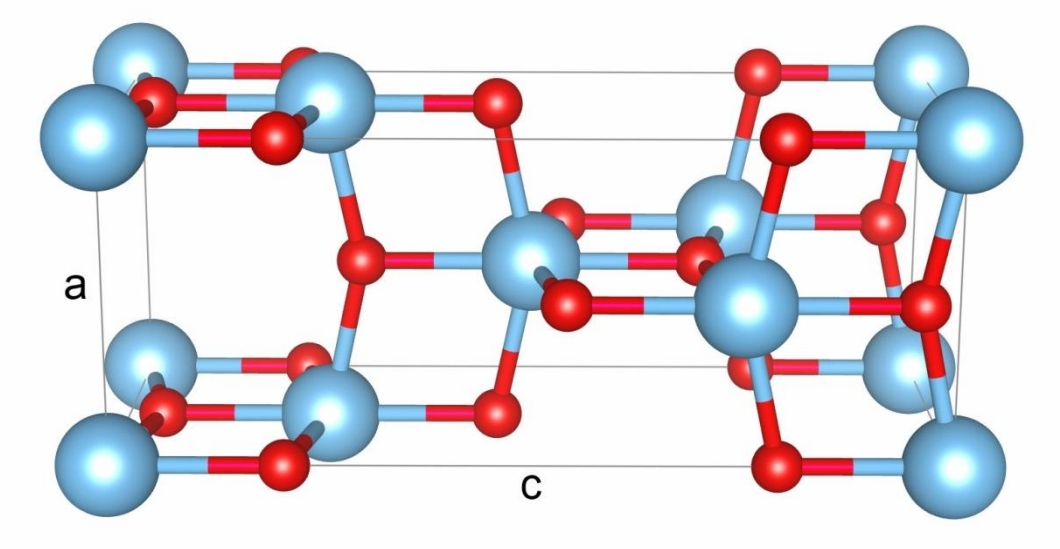


Figure 1: Ball-and-stick model of an anatase unit cell. Ti atoms are blue, O atoms are red.

For the study of particular surfaces, high quality single crystals are required, which are difficult to acquire in the case of anatase. Often natural samples are used, but usually unknown impurities with concentrations up to several percent are present. While samples can be analyzed rather accurately with methods such as inductively coupled plasma mass spectrometry (ICP-MS, sensitivity of ppm or better), this does not consider preferred accumulation of impurities either on the surface or in the bulk. Surface sensitive techniques such as x-ray photoelectron spectroscopy or Auger electron spectroscopy have a detection limit of 0.1-1% of the surface layer, which makes identification of defects frequently found in STM difficult [23]. Due to impurities and other defects, natural crystals often deviate from the calculated density in Table 1.

The creation of (usually sub-)mm sized synthetic single crystals is also possible using chemical transport reactions [24]. This has the advantage of known dopant levels, but handling of these small crystals can be difficult.

The frequent occurrence of anatase in nanocrystalline $TiO_2$ powders such as Degussa P25, which consists of 75% anatase and 25% rutile [17], can possibly be attributed to the low surface energy of equilibrium-shape anatase crystals (Figure 2), even though the lowest energy of any $TiO_2$ surface is that of rutile (110) [19, 25].

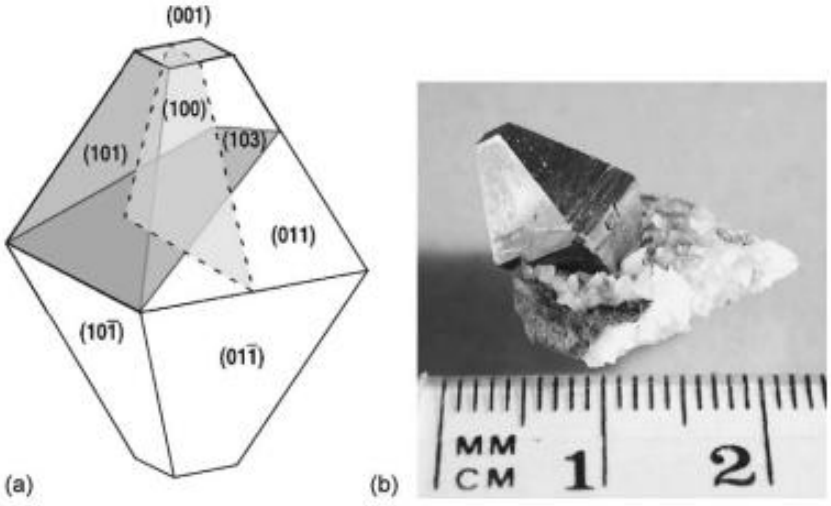


**Figure 2: Wulff construction (a) and photo (b) of an equilibrium-shape anatase crystal, image taken from ref. [19]**

### *1.1.2.1 The (101) surface*

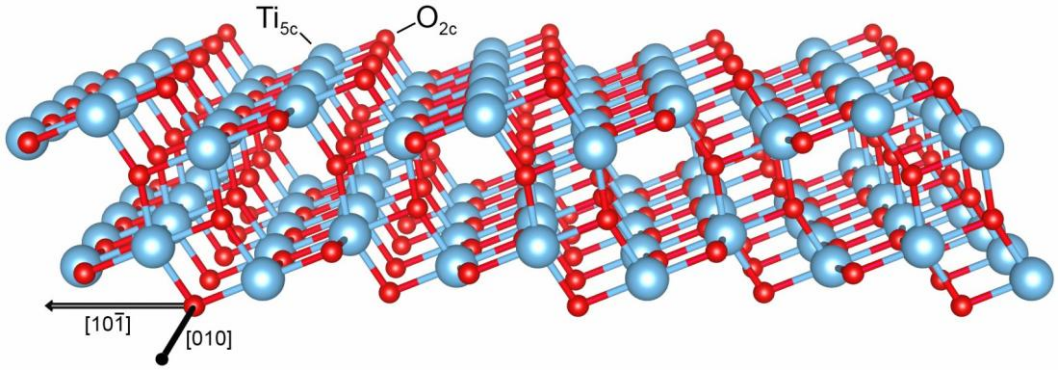


**Figure 3: Ball-and-stick model of the anatase (101) surface. Positions of low coordinated $Ti_{5c}$ and $O_{2c}$ atoms are marked, the other surface atoms have bulk coordination ($Ti_{6c}$ and $O_{3c}$).**

The (101) plane is the most stable one of anatase, making more than 94% of the surface in the Wulff construction [18]. An interesting property of the (101) surface is the fact that it does not show any surface oxygen vacancies ($V_O$) at room temperature [26], which is uncommon for a reducible metal oxide. The reason for this is that next to a surface $V_O$ a doubly undercoordinated $Ti_{4c}$ site is formed, which is energetically unfavorable when compared to a subsurface $V_O$ [19, 27]. This is also why subsurface $V_O$s are more stable below $Ti_{6c}$ surface sites rather than at the position below a $Ti_{5c}$ site as this would again lead to $Ti_{4c}$.

The ball-and-stick model in Figure 3 displays the sawtooth-like structure of the (101) surface, which consists of undercoordinated (2c, 5c) as well as of bulk-coordinated (3c, 6c) O and Ti atoms. Figure 4 shows a typical anatase (101) surface as imaged in STM. In the right image bright and dark areas are visible, which are attributed to band-bending induced by charged subsurface defects [28]. The ovals in "atomically-resolved" STM images represent pairs of $Ti_{5c}/O_{2c}$ atoms.

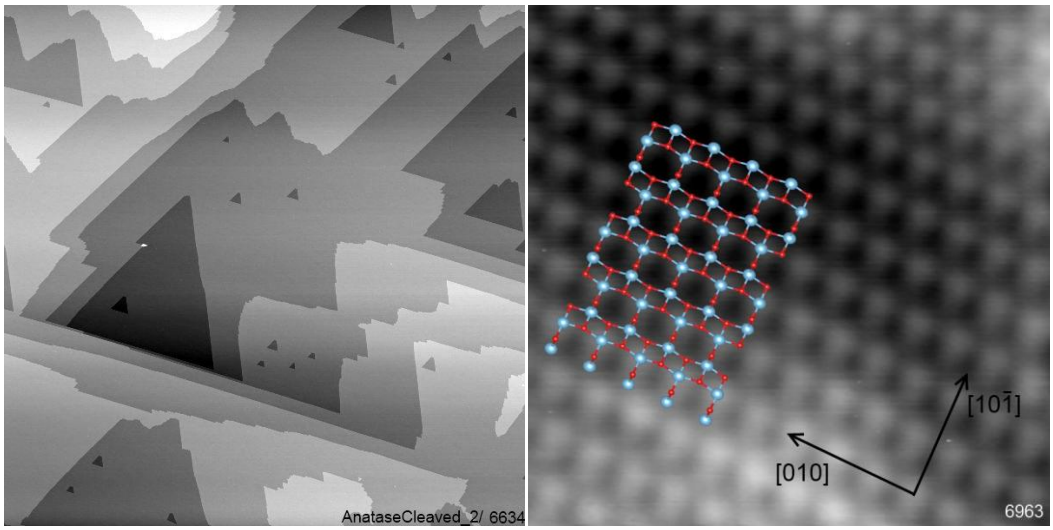


**Figure 4: STM images of the clean anatase (101) surface (natural sample). Left: 1×1 µm$^2$, +1.5 V sample bias, 0.06 nA. Large scale image showing the typical triangular terrace shapes. Right: 3.5×3.5 nm$^2$, +1 V, 0.08 nA. High resolution image with a surface model overlaid. The surface orientation is according to [29]. Image orientation is the same in all images in this work.**

# 2 Experimental

## 2.1 UHV setup

All experiments were performed in an Omicron LT-STM (low-temperature scanning tunneling microscope) UHV (ultra high vacuum) setup (drawing in Figure 5). The system consists of two UHV chambers, separated by a valve, with ion pumps and titanium sublimation pumps in each chamber. One is the preparation chamber which contains equipment necessary for sample preparation. This includes:

- Ion gun
- Electron gun
- LEED
- Electron beam heating station (up to 900°C)
- Quadrupole mass spectrometer
- Leak valves
- Tungsten wire for hydrogen cracking

Transfer between the chambers is done by a manipulator that can be heated up to 700 K and cooled by liquid nitrogen down to 100 K.

The other chamber, the analysis chamber, contains the sample storage, the STM with the cooling system and a leak valve for gas dosing directly into the STM head. The cooling system consists of two cryostats, the outer one is filled with liquid nitrogen and the inner one can either be filled with liquid nitrogen or liquid helium. To perform measurements at temperatures that cannot be reached directly by this cooling (78 K with nitrogen and 6 K with helium), additional heating of the STM is possible but was not used in these experiments. To minimize vibrations, which is necessary in experiments where height differences of pm need to be detected, the STM head is equipped with spring-suspension with eddy current dampening. Vibrations are further reduced by pneumatically lifting the whole UHV chamber.

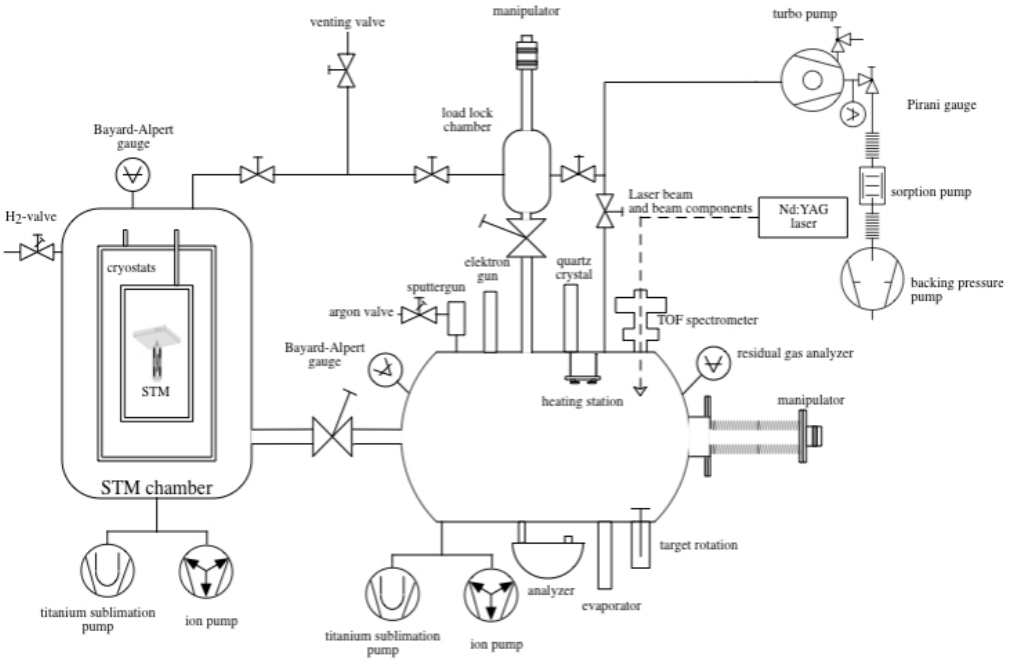


Figure 5: Schematic drawing of the LT-STM chamber. Image taken from [30]

## 2.2 Scanning tunneling microscope

### 2.2.1 Theory

In a scanning tunneling microscope (STM) a sharp and conductive tip is approached very close (about half a nm distance) to a conductive sample. A bias voltage, usually between 0.01 V and 5 V, is applied between sample and tip, which leads to a tunneling current in the nA range. This is due to the exponential decay of the quantum mechanical wave function in classically forbidden regions (tunneling effect). In a one-dimensional approach this can easily be shown by solving the time independent Schrödinger equation for a potential barrier.

$$\left( -\frac{\hbar^2}{2m}\frac{\partial^2}{\partial x^2} + V \right)\psi(x) = E\psi(x)$$

A rectangular barrier of height $\phi = V - E$ and width ***d*** is assumed (for electrons near the Fermi edge) and leads to a transmission $T \propto e^{-2\kappa d}$ with $\kappa = \sqrt{\frac{2m\phi}{\hbar^2}}$

The transmission, and thus the tunneling current, depends exponentially on the barrier width d, which leads to a high sensitivity to height differences. It should be noted that the actual (geometrical) height cannot be measured, but rather a convolution of tip-sample-distance, d, and the local electronic density of states.

In order to create STM images, two methods are commonly used. In the constant current mode, the tip is scanning the surface with a feedback loop that adjusts the tip height so that the tunneling current remains constant. The image is then created from the height adjustments of the tip. The second method is the constant height mode where the feedback loop is turned off or very slow, and the image is created from the current. While this often gives better images, there is imminent danger of crashing the tip at step edges or on other asperities on the surface when the feedback loop is turned off completely.

While STMs in principle also work under atmospheric pressure, they are usually operated in ultra high vacuum (UHV) with pressure below $10^{-9}$ mbar. This is necessary to reduce contamination of the surface, as at $10^{-6}$ mbar every surface atom is hit by roughly one residual gas atom per second on average. A special kind of STM, the electrochemical STM, operates in high purity electrolytic solutions and is used to observe reactions of ions in the electrolyte with the surface [31, 32].

### 2.2.2 Setup

#### *2.2.2.1 Tip movement*

In the following description it is assumed that the tip is moved while the sample is stationary, but moving the sample while having a fixed tip instead is also a common way.

An STM tip has to be moved over relatively large distances of a few mm, yet with a high precision in the range of picometres. This is implemented by using two different systems, dividing tip movement into coarse motion with steps of several hundred nm and high precision fine motion with a range around 1 µm. Both kinds of motion systems are based on piezoelectric elements, which deform when a voltage is applied between two different points.

##### *Coarse motion*

Coarse motion is done in steps using so-called stick-slip motion. For this, the tip is held on shear mode piezos (labeled “stacks” in Figure 6) only by friction. When the piezos move slowly (stick part of the motion, shallow slope in Figure 6), friction is strong enough to move the tip, while with faster movement inertial forces hold the tip roughly in place (slip part, steep slope).

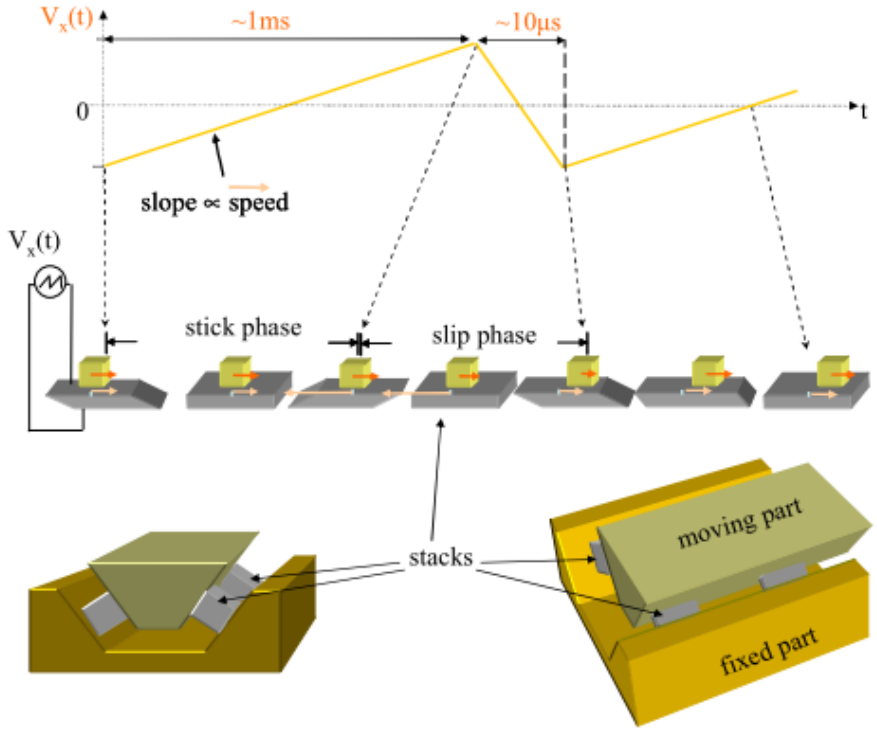


Figure 6: Stick-slip-movement. The stacks are glued to fixed part. Image taken from [33]

### *Fine motion*

For fine motion, the tip is mounted on a small tube scanner made of a piezoelectric material. With electrodes arranged as in Figure 7, the scanner can bend in any direction and contract/expand, allowing precise positioning of the tip.

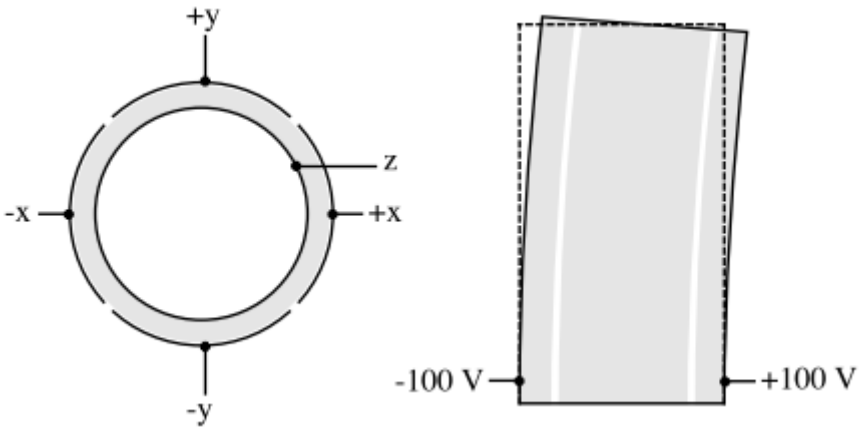


Figure 7: Piezo tube scanner, image taken from [23]

#### *2.2.2.2 STM tips*

STM tips are usually made of tungsten or a platinum-iridium alloy, but other materials such as gold are sometimes also used. To get small tips with a desired radius of a few nm

(ideally with one atom on top) they are electrochemically etched from a wire, although mechanical methods of preparation such as grinding or cutting are possible [34, 35].

All tips used in this work have been electrochemically etched from a 0.5 mm tungsten wire in a thin film of 5% KOH solution and mounted on a tip holder for transfer and usage inside the chamber. Once inside the UHV system, tips are sputtered with 3 µA $Ar^+$ ions with 3 keV ion energy for 30 min in order to remove the oxide layer that forms on tungsten under ambient conditions. The total sputtered area is 5×8 $mm^2$, which leads to $8.4\times10^{16}$ ions/$cm^2$. Before scanning the sample, the tip condition is improved by scanning a gold (110) single crystal. During this treatment, the gold surface is slightly touched with the tip and voltage pulses of 4-6 V are applied. This stabilizes the tip because a small amount of gold stays on the tip, making it inert to reactions with residual gases and adsorbates on the sample.

## 2.3 Samples

Two different samples were used in this work, one natural and one synthetic crystal. A part of the $CO_2$ experiments (chapter 3.3) were done on the latter one, everything else was done on the natural sample.

### 2.3.1 Natural sample

The natural anatase crystal was cleaved to obtain a nice (101) surface. While the sample (overlaid by blue and red frames in the left image of Figure 8) is about 1.7×4.8 $mm^2$ in size, only the small 1.7×0.7 $mm^2$ region marked in red was used for the experiments. This was mainly done because this region is rather far away from the sample mounting, which avoids having present sputtered tantalum from the mounting on the scanned surface. Another reason for mainly scanning in the red region is that it is rather flat. Often terraces of several hundred nm are found, but also some regions with higher step density (Figure 9).

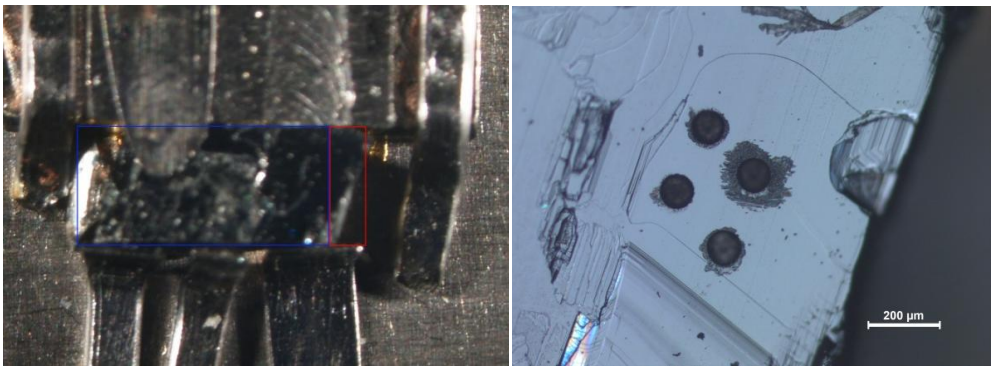


**Figure 8: Photograph of the natural sample. Left: The whole sample with mounting. All STM images were taken on the area framed in red. Right: The most commonly scanned area with holes left from ICP-MS analysis. Photograph from research group Inorganic Trace Analysis.**

In STM images of the sample, a very common type of defect can be found (see Figure 10, right image), which was later identified as a Nb atom taking the place of a $Ti_{6c}$ surface atom (supplement of [36], model in the left image of Figure 10). Identification was possible after an elemental analysis (results in Table 2) using inductively coupled plasma

mass spectrometry (ICP-MS), which was done by the research group Inorganic Trace Analysis, Institute of Chemical Technologies and Analytics. During the analysis, 4 holes with a diameter of 80 µm each were made in the usually scanned area using a laser (Figure 8, right).

| Element | Amount (% weight) |
|---|---|
| $^{24}$Mg | 0.043 ± 0.003 |
| $^{65}$Cu | 0.31 ± 0.07 |
| $^{66}$Zn | 0.74 ± 0.04 |
| $^{93}$Nb | 1.24 ± 0.1 |
| $^{115}$In | 0.005 ± 0.003 |

**Table 2: Impurities found in the natural sample**

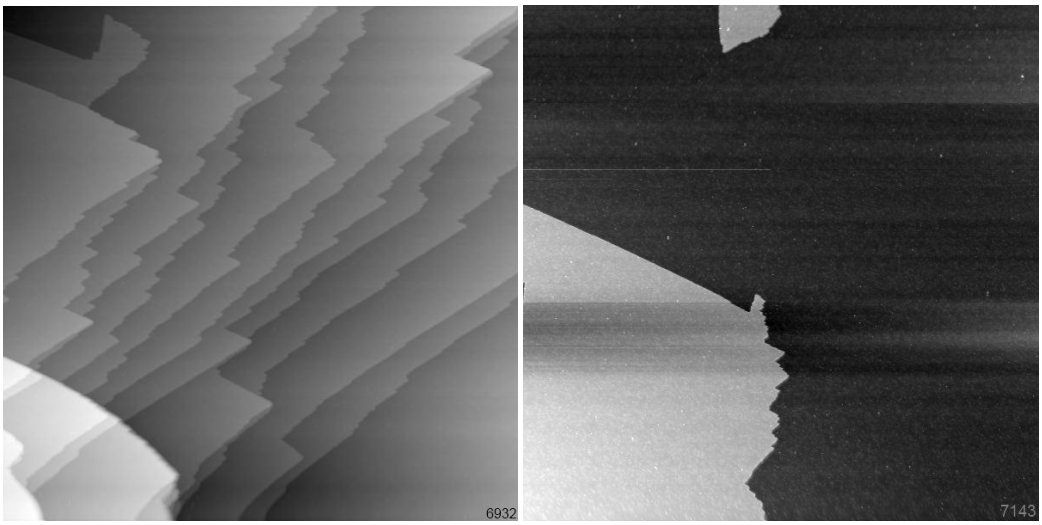


**Figure 9: Left: 300×300 nm$^2$, +2 V, 0.1 nA, high step density area. Right: 500×500 nm$^2$, +2 V, 0.1 nA, low step density area. Both areas area are part of the usually scanned region. Much higher step densities can be found elsewhere on the sample.**

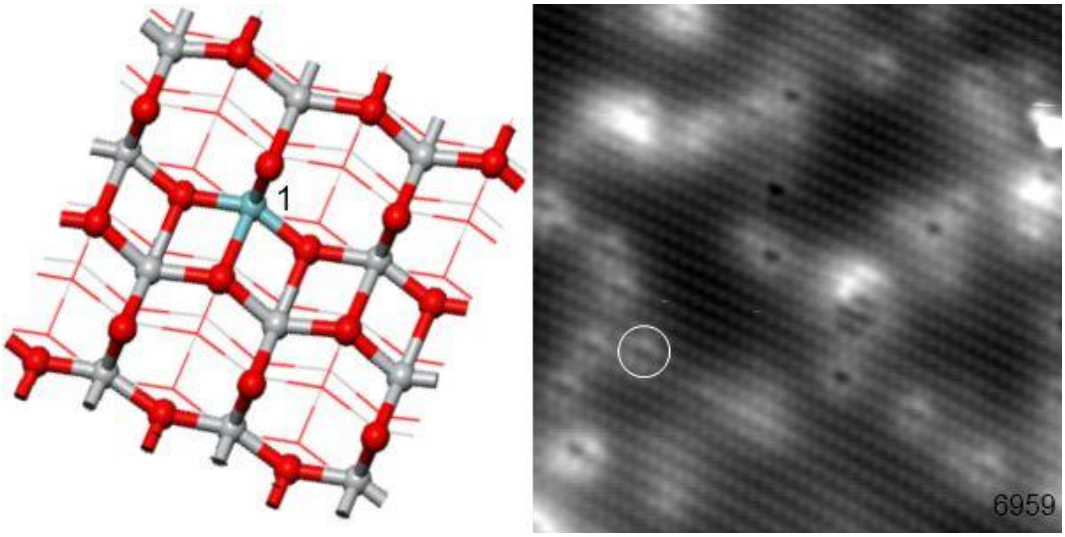


**Figure 10: Left: model of a Nb atom replacing a $Ti_{6c}$ atom at position 1 (image taken from supplementary materials of ref. [36]). Right: 15×15 nm$^2$, +1.5 V, 0.08 nA, Nb appears as point-defect surrounded by a bright area (marked by the white circle).**

### 2.3.2 Synthetic sample

The other sample used for experiments is a synthetic crystal grown by chemical transport reactions employing $TeCl_4$ as the transporting agent [24]. In the growth process the sample was doped with about 0.3% Al. No trace element analysis was done, but for the crystal grown as in [24], the dopant levels are expected to be very similar.

The sample is roughly 1.5×1 $mm^2$ in size and initially was transparent without any shade of color (Figure 11) and not conductive enough for STM and LEED measurements. Treatment to make the sample suitable for STM is described in chapter 2.4.3.

**Figure 11: Photograph of the synthetic sample mounted on an 18×15 $mm^2$ omicron Ta sample plate. The materials used for the holder are Ta and Au.**

As the sample is very small, mounting the sample with a simple clip on top was not possible. Instead it was pressed from the side. Consideration was given to avoid sputtering Ta from the clip onto the surface. Small gold plates were placed between the sample and the clip to improve thermal contact to the sample plate and to reduce mechanical stress on the sample that could lead to cracking. While the mounting was not done perfectly (see Figure 12), a reasonable part of the sample was in a position far enough above the clips to have only a small amount of Ta sputtered on it.

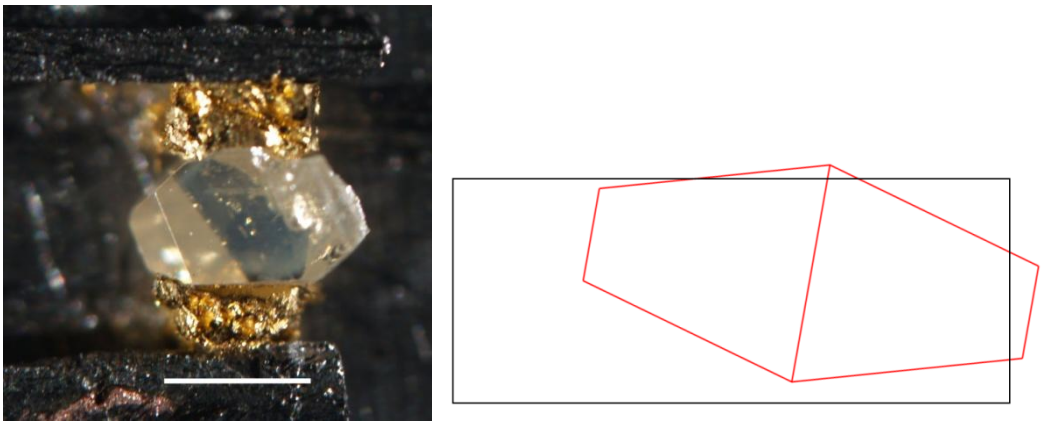

**Figure 12: Left: Photograph of the synthetic sample with a scale bar (1 mm). Right: Schematic drawing of the sample (red) and the Ta clips (black) in side view.**

STM images revealed a rather rough surface with many small terraces (top left image of Figure 13). The long straight step edges and triangular terrace shapes typical for anatase were found to occur less frequently than on the other samples. The synthetic sample showed more round step edges. Different to other samples, bulk defects such as the screw dislocation in the top right image of Figure 13 were found several times.

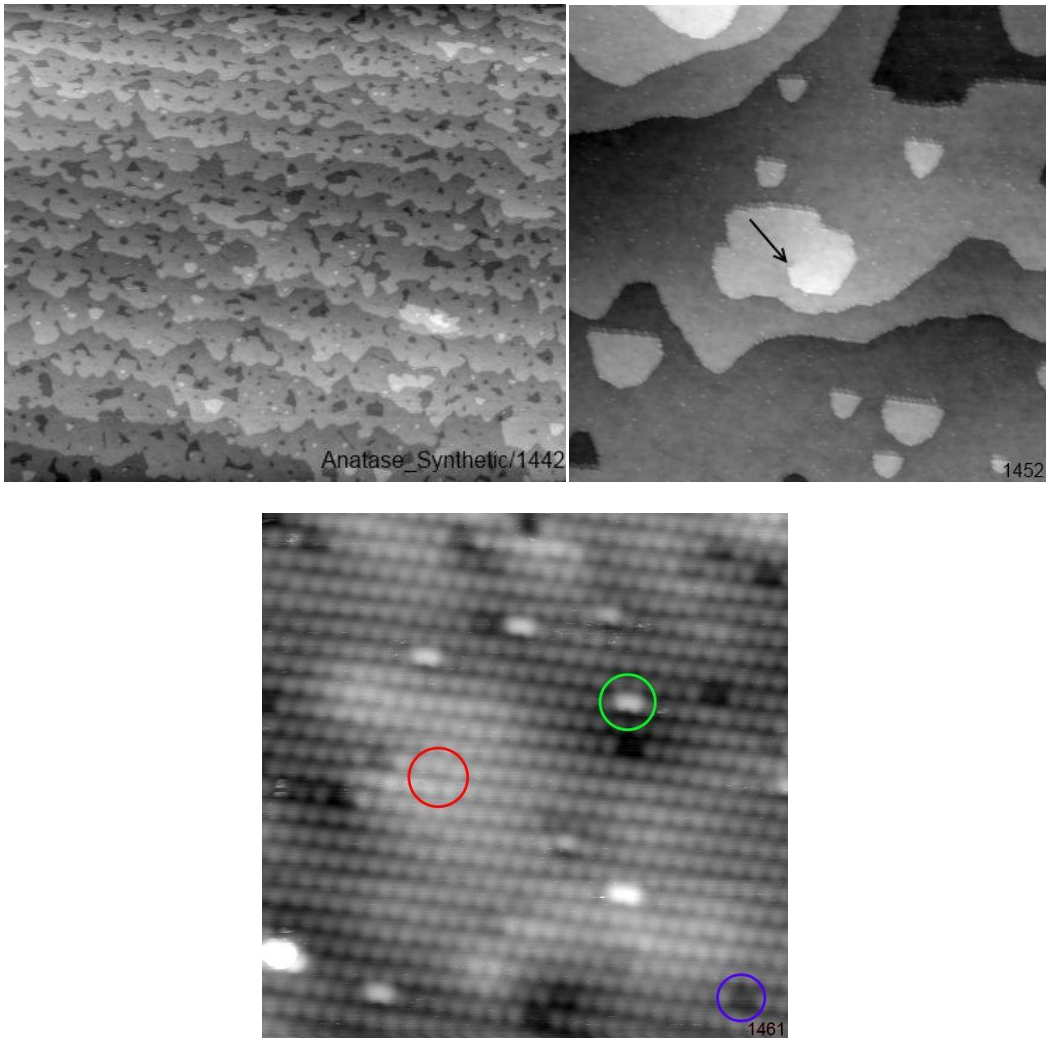


**Figure 13: Typical STM images of the synthetic sample. Top left: 1000×850 nm$^2$, +3 V, 0.06 nA, large scale image, in some regions more regular terrace shapes are found. Top right: 150×150 nm$^2$, +1.8 V, 0.1 nA, screw dislocations (marked by an arrow) are relatively common. Bottom: 10×10 nm$^2$, +1.2 V, 0.07 nA, high resolution image showing defects typical for the synthetic sample: Dark triangles (blue) might come from Al, bright spots (green) are probably sputtered Ta and a defect similar to the Nb defect on the natural sample (red).**

STM images with atomic resolution (Figure 13 bottom) show dark defects (blue) that might be caused by the 0.3% Al content of the sample, and a brighter type of defect (green). The amount of the bright defects varies slightly with sample preparation and strongly with the location of the scanned area on the sample, making it a candidate for sputtered Ta. A defect of the same type as the one attributed to Nb in the natural sample (red) is also found, albeit rather rarely.

On the anatase (101) surface it is possible to create surface $V_O$s by scanning with STM at high bias [36]. While on several investigated natural samples the threshold bias voltage

for creation of surface $V_O$s was around 5.5 V, at least 7 V are required for the same effect on the synthetic sample. This difference is likely to originate from the less reduced state of the synthetic sample when compared to natural ones, as the surface $V_O$ creation is done by field induced migration of subsurface $V_O$s towards the surface [36].

## 2.4 Sample preparation

### 2.4.1 Typical cleaning cycle

Prior to experiments, the sample is sputtered in $2\times10^{-6}$ mbar Ar pressure by 1 kV $Ar^+$ ions for 10-15 min and annealed to 720°C for 10 min. Sometimes a second cycle was performed if the sample did not seem clean enough in STM. The sputter current was between 0.8 and 1.4 µA, with a sputtered area of 6×5 $mm^2$, which means a total dose of $10^{16}$ to $2.62\times10^{16}$ $Ar^+$ ions per $cm^2$.

In order reduce the number of Nb defects on the surface, it was found helpful to let the sample cool down below 400°C after annealing and then anneal it for 10 more minutes to 700°C. This cool down and annealing is repeated for temperatures of 680°C and 660°C.

### 2.4.2 Reoxidation

Since oxygen is preferentially sputtered, the sample becomes more and more reduced with an increasing amount of sputter cycles. To counter this, the sample is reoxidized roughly every 10-15 sputter cycles. This is done by annealing to 430-500°C in $5\times10^{-7}$ mbar oxygen pressure for 10-20 min immediately after sputtering. The sample is then sputtered again, starting the normal cleaning cycle mentioned above.

### 2.4.3 Initial treatment of the synthetic sample

After the initial 3 sputter/anneal cycles, the synthetic sample was not conductive enough for STM and LEED below 80 eV electron energy. In order to reduce the sample for increasing its conductivity, it was moved to another UHV setup (PINUP) to perform more extensive sputtering. This allowed easier repeatable cleaning cycles as the sample did not need to be moved between sputtering and annealing positions. In addition, the sputter gun was better focused than the one in LT-STM, which made it possible to sputter just the crystal without the risk of sputtering material from “higher” parts of the clip onto the sample.

The synthetic sample was sputtered with 1 keV $Ar^+$ ions in $2\times10^{-7}$ mbar Ar pressure with a sputtering current of 65 nA. Each sputtering cycle lasted for 60 min, yielding a total dose of $9.75\times10^{16}$ $Ar^+$ ions/$cm^2$, followed by 10 min annealing at roughly 600-650°C. Due to a bad thermal contact to the thermocouple the temperature had to be roughly judged by the glow of the sample plate, which becomes visible above 600°C. After 8 cycles and one additional cycle with 30 min annealing, LEED patterns were visible down to 40 eV and the sample was moved back to the LT-STM chamber.

Probably because of reoxidation during the sample transfer under ambient conditions, there was once again no LEED pattern visible below 80 eV. However, this was quickly resolved by several more sputter/anneal cycles at 1 and 2 kV. At this point, STM measurements were possible. It was noticed that the sample had acquired a slight

yellow tint during the sputtering cycles, which did not change over the course of the experiments.

## 2.5 Dosing

During the experiments, various materials were dosed on the surface and investigated in STM. The ways of dosing each of the substances is described in the following. All coverages in this work correspond to the number of $Ti_{5c}/O_{2c}$ pairs; an anatase (101) surface unit cell has two of these ($6\times10^{14}$ pairs per $cm^2$).

### 2.5.1 $CO_2$

$CO_2$ was dosed directly into the STM head with the sample cooled by liquid helium. This is necessary because, when dosing $CO_2$ at temperatures above 78 K, there were no new adsorbates visible in STM images, although, according to TPD measurements, it should still be on the sample [37, 38].

### 2.5.2 $O_2$

Oxygen was dosed either directly into the STM head or by cooling the manipulator to 100-115 K and filling the preparation chamber with $1\text{-}5\times10^{-7}$ mbar $O_2$.

The important difference between the two ways of dosing is that at 100 K the only $O_2$ molecules that stick are located on top of Nb defects, while dosing $O_2$ directly into the STM head at 78 K allows oxygen to adsorb at any normal surface site.

### 2.5.3 Hydrogen

Atomic hydrogen was dosed by cracking molecular $H_2$ in a catalytic reaction using a 1600-1700°C hot tungsten filament close to the sample [39] (initially 5 cm). For this the preparation chamber was filled with $10^{-7}$-$10^{-6}$ mbar of $H_2$. The relatively high amount of $H_2$ required for a sufficient amount of atomic H onto the surface makes this method quite sensitive to impurities in the $H_2$ gas, which are in the range of 10-50 ppm. During the initial experiments this caused some problems, but reasonable contamination levels were obtained when a new W filament was positioned at 3-4 cm from the sample. Atomic H was dosed at different sample temperatures ranging from 100 K to 310 K.

### 2.5.4 Water

$H_2O$ was dosed by filling the chamber with $10^{-9}$ mbar water with the sample in the cold (100-150 K) manipulator. While dosing directly into the STM would also be possible, this was not done to avoid water contamination of the analysis chamber. Isotopically labeled water (with $^{18}O$) was used instead of the usual $^{16}O$, but it is expected that using “normal” water does not cause any significant changes to the results. (This was done because there was no other source of highly purified water available at the time of the experiments.)

## 2.6 Electron bombardment

In order to create surface $V_O$s, the sample was exposed to a 500 eV electron beam. In a process known as the Knotek-Feibelmann Mechanism [40] these electrons are able to desorb surface oxygen atoms. This is a common technique for creation of surface $V_O$s on $TiO_2$ anatase, which otherwise do not occur naturally [2].

The electron beam used for $V_O$ creation was scanned over an area of 3×2 $mm^2$ on and around the area of interest on the natural sample. With a measured current of -1.5 µA (not considering secondary electron emission) for a time of usually 5 min, this leads to an electron dose of $5.1\times10^{16}$ electrons/$cm^2$. To minimize emission of secondary electrons and adsorption of ionized atoms or particles that might be desorbed by electrons, the sample is put on a potential of +27 V. During and after electron bombardment the sample is cooled to 100-115 K to avoid migration of the $V_O$s to the subsurface as it usually occurs above 200 K [2].

# 3 Results

## 3.1 Water

On the typically defect free anatase (101) surface water adsorbs in a molecular fashion [41]. According to prior research [41, 42], water desorbs slightly below room temperature from anatase (101), but some stays at room temperature above subsurface defect sites [41]. For temperatures below 130 K, a sticking coefficient of 1 is reported in [42]. Dosing at different temperatures indicates that there is no change at higher temperatures at least up to 170 K. This can be expected from the low coverage TPD spectra in [42] where desorption starts around 225 K.

Work on water was performed for two reasons. First, water is a common contaminant in $H_2$, so when dosing hydrogen at low temperatures getting water on the sample cannot be avoided. The second reason is that water offers an alternative path of getting atomic hydrogen onto the surface: First, surface $V_O$s are created by electron bombardment as described in chapter 2.6, then water is dosed onto the sample. When a water molecule encounters a $V_O$ it dissociates as calculated in [43]. Similar to the rutile (110) surface [20], the oxygen atom fills the $V_O$ while the hydrogen atom binds to a neighboring bridging oxygen site. This dissociative adsorption is common on rutile (110), because there are usually surface $V_O$s present after preparation, while on near perfect rutile (110) only molecular $H_2O$ adsorption is found [1, 44].

All water experiments were done on the natural sample. Only a few different water exposures were performed, all at temperatures where a sticking coefficient of 1 is expected. After dosing at room temperature, no water was found on the surface. Figure 14 shows a typical STM image of water on the anatase (101) surface. While $H_2O$ is reported to be adsorbed stronger above subsurface defects, no preferred adsorption sites were found.

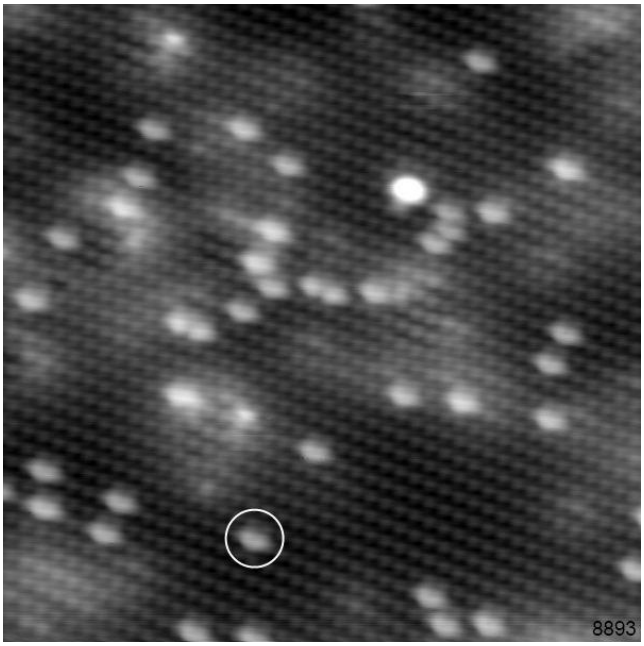


**Figure 14: 15×15 nm$^2$, 1 V, 0.1 nA, water (0.009 L, 2.1% coverage) dosed on the natural sample. $H_2O$ (marked by a white circle) exhibits a typical, somewhat star-like, shape.**

An initially surprising trend is seen in the data in Figure 15. One would expect that twice the dose would double the coverage, as in this temperature regime a sticking coefficient of 1 is valid even for multilayer adsorption [42]. Instead there is an offset of approximately 1% coverage when extrapolating the least squares fit in Figure 15 to 0 L. This is likely to be caused by adsorption of residual water after dosing, as the water pressure in the chamber decreases rather slowly.

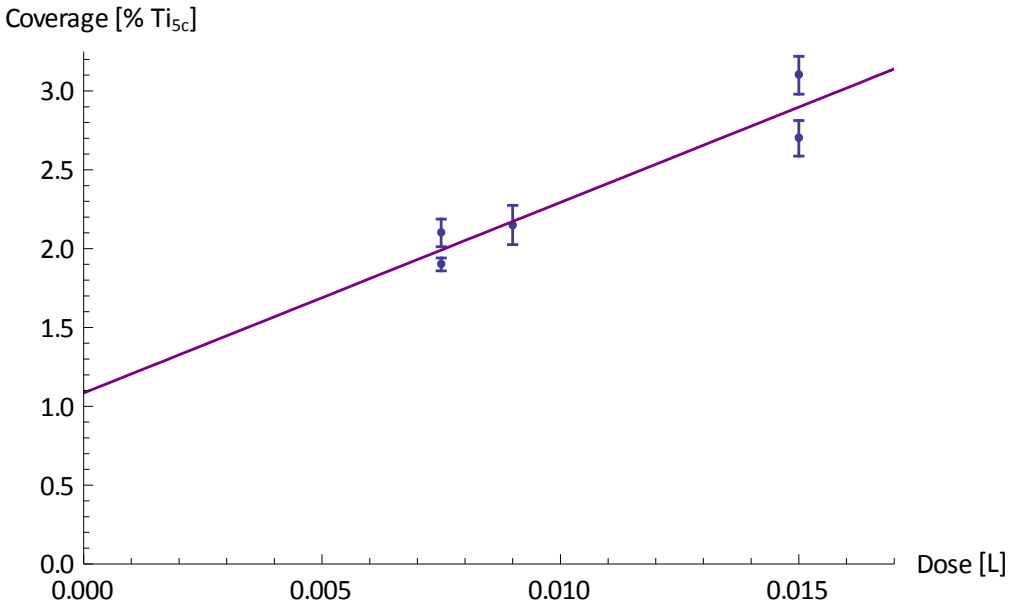


**Figure 15: Water coverage versus dosed amount with a linear least squares fit. The offset might come from adsorption of residual water.**

Calculations in [41] show that water is expected to bond with the O atom to a $Ti_{5c}$ site and with each of the H atoms to a $O_{2c}$ site as shown in Figure 16 (left). Simulated constant electron density images are in fair agreement with measurement results (Figure 16 right).

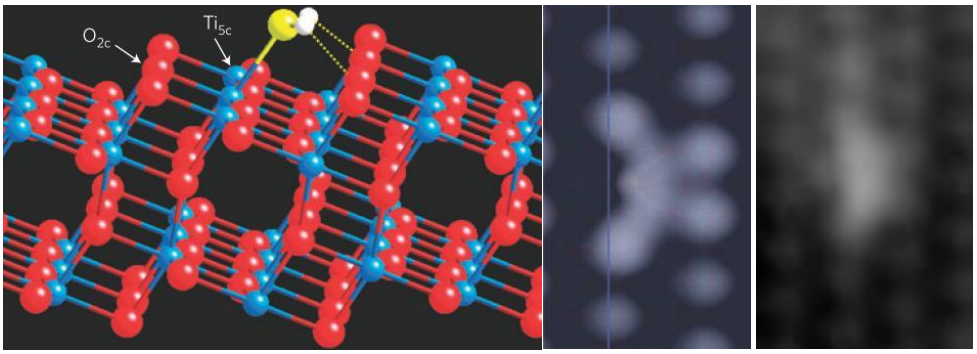


**Figure 16: Adsorption position (left, taken from [41]). The simulated (middle, taken from [41]) and measured (right) STM images of molecular water fit quite well.**

Water was dosed up to a coverage of 3% of the surface $Ti_{5c}$ atoms. Dosing more water was attempted, but with increasing coverage the image quality rapidly decreased. Already at 3% a stable tip and sufficient image quality was found rather difficult to achieve.

### 3.1.1 Thermal stability

A short survey of the behavior of water at different temperatures was taken and found to be consistent with the low coverage TPD spectrum in [42] where the water desorption peak is located between 225 K and 320 K with a maximum at 260 K. It should also be noted that, according to DFT calculations, water is bound 0.3 eV stronger above a subsurface $V_O$ [45] which might lead to somewhat different behavior dependent on sample preparation (number sputter cycles and time since last reoxidation). While it is immobile at 78 K, in [41] it is reported that at 190 K water diffuses on the surface, mostly along and in rare cases across the rows. This is in agreement with the results in chapter 3.2.1.2, where water has to diffuse in order to undergo the observed recombination with $V_O$s after annealing to 210 K, leaving two neighboring H atoms behind. After annealing a surface with 2% $H_2O$ coverage to 290 K for 10 minutes, no water could be found anymore.

### 3.1.2 Tip interaction

At the usual scanning temperature of 78 K, water was found to be stable and immobile at low bias voltages. High bias irreversibly changes the water molecule; a bias above 3.5 V always converts $H_2O$ into a bridging oxygen dimer (Figure 17 **E**). In a narrow and somewhat tip-dependent bias range, usually between 3 and 3.5 V, water is converted into an intermediate state (Figure 17 **C**). While 78 K, there is no stable bias for certain conversion into the intermediate state, it works much better at the temperature of 6 K that was used in Figure 17. Sometimes a two-step-conversion is observed (Figure 18, blue circle), where the newly created intermediate state is further converted into a bridging oxygen dimer just a few scan lines later. This dimer is a feature where two oxygen atoms occupy the position of a single $O_{2c}$ surface atom [36]. The intermediate state is assumed to be a terminal hydroxyl group (OH). This comes from an appearance that is similar to $H_2O$, as OH is expected to bind to a $Ti_{5c}$ site [46]. Another hint is the similar bias for conversion from $H_2O$ to OH and from OH to a bridging dimer, indicating removal of the hydrogen atoms in a one by one fashion.

As with atomic hydrogen (see chapter 3.2.2) the H removed during the conversion is assumed to go to the STM tip, which can attract $H^+$ ions due to its negative bias relative to the sample. Desorption as molecular $H_2$ can be ruled out by the observed one by one removal of H.

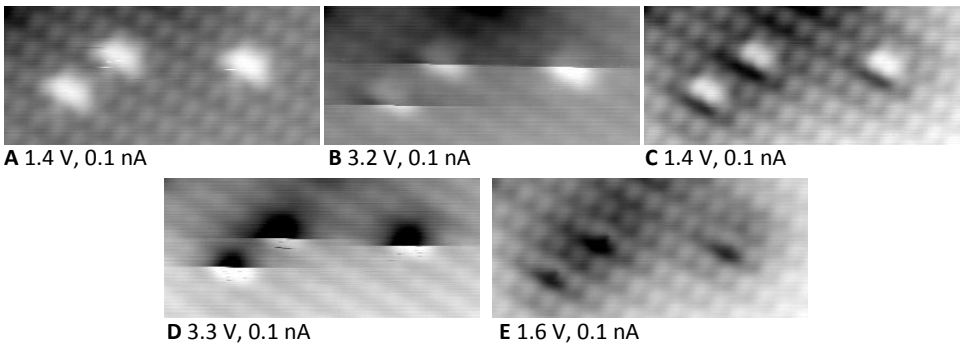


**Figure 17: 3.9×1.7 nm², 6 K. Water is converted into OH by a 3.2 V scan (B) and further converted into bridging oxygen dimers by scanning at 3.3 V (D). Images taken from ref. [36].**

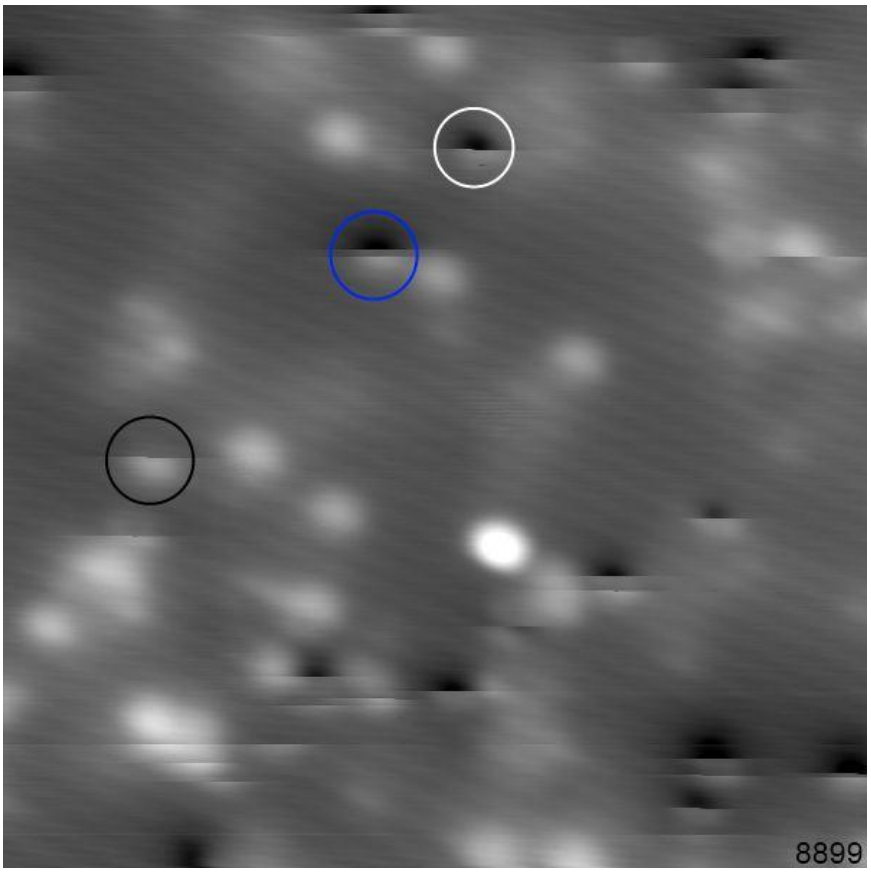


**Figure 18: 15×15 nm$^2$, 3 V, 0.1 nA, 0.009 L water (2.1% coverage). Water is converted by high bias: directly into a bridging dimer (white), into a bridging dimer with OH intermediate state (blue), into OH (black).**

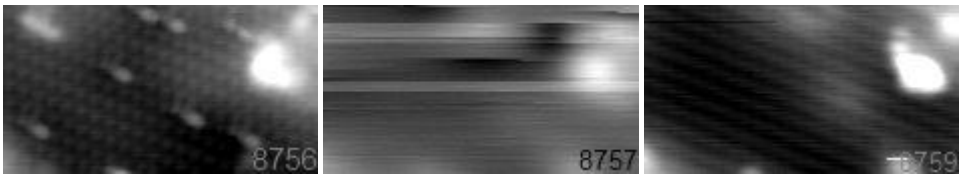


**Figure 19: 8×4 nm$^2$, 1 V, 0.1 nA, water (0.015 L, 3.2% coverage) was converted into bridging oxygen dimers (left image) by a prior 4 V scan. These are removed by a 5 V scan in the middle image.**

While usually immobile, water can be moved by the tip over short distances during a scan above 3 V on very rare occasions. Movement happens more often in a combination with conversion of the water molecule into OH or a bridging oxygen dimer. Scanning at an even higher bias of 5 V removes the bridging dimers (Figure 19 and Figure 20), whereby the additional O atom moves into the bulk to fill a subsurface $V_O$ [36].

Although usually bias voltage is mentioned when changing water into bridging dimers, it seems that actually the electric field is the important factor. This indicated by the STM image in Figure 20 where a rather large area around the 20×20 nm$^2$ central area, scanned at 5 V, shows the dark band bending indicative of bridging dimers. There is also a big area of dark band bending visible extending about 20 nm above the scanned area that presumably reflects the tip shape as sketched in Figure 20.

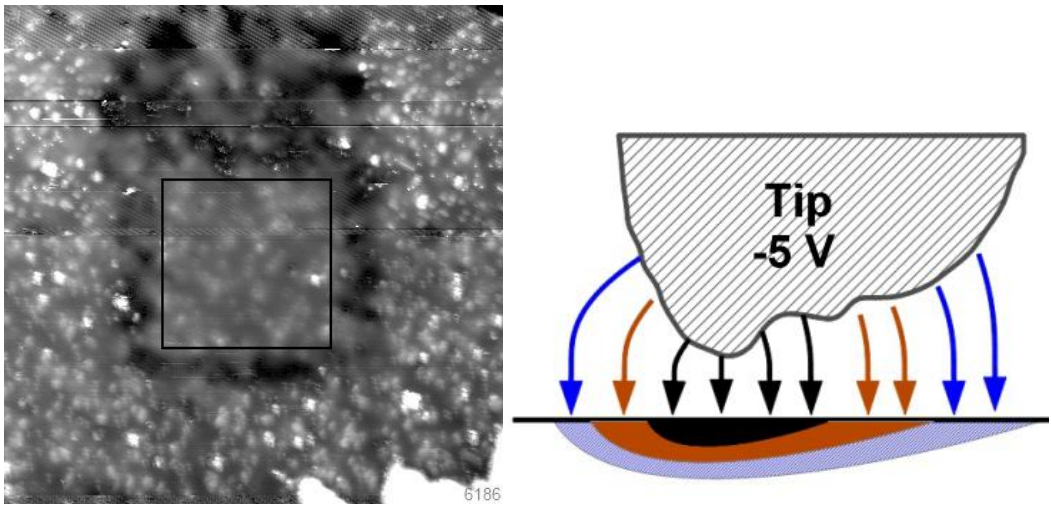


**Figure 20: left: 60×60 nm$^2$, 1 V, 0.15 nA, water (2.7% coverage). The central area marked with a square was scanned at 5 V before, removing all $H_2O$, OH and bridging dimers. Even outside the scanned area water is converted into bridging dimers (dark area), which shows the importance of the electric field for the conversion. The large black area "above" the scanned area comes from an asymmetric tip. Right: sketch of an asymmetric tip, black: scanned area, bridging dimers removed, brown: water converted into bridging dimers, blue: field too weak for conversion.**

### 3.1.3 Changes in behavior with $O_2$ on the surface

In chapter 3.1.1 it was reported that all water desorbed when annealing above 290 K. However, with $O_2$ adsorbed on the surface, the behavior of $H_2O$ was found to be different. On the flat surface and above 78 K, molecular $O_2$ adsorbs exclusively at Nb defect sites, forming the so called "bright dimer" (marked red in Figure 21).

Figure 21 shows data from an experiment where both, $O_2$ and $H_2O$, were dosed on a surface. The treatment steps are summarized in Table 3. First 0.015 L water was dosed at 130 K, then additional 0.0375 L $O_2$ was dosed into the cryostat (Figure 21 **A** and **B**). After annealing to 290 K for 10 min it was found that all the remaining water had changed into OH. The coverage of water, and OH, went down from initially 3% to 1.1%, respectively, and the bright dimer $O_2$ coverage changed from 0.8% to 0.2%.

In Figure 21 **C** a rather uneven distribution of the OH can be seen, which is in contrast to the positions of the water molecules before annealing (Figure 21 **A** and **B**). The reason for this is not clear, but regions with certain subsurface defects or proximity to other OH groups might be energetically favorable for OH. An alternative explanation would be interaction of the diffusing water with the $O_2$ molecules adsorbed on the Nb defects, where 2 $H_2O$ molecules and one bright dimer might be converted into 4 OH groups. As the OH is stronger bound to the surface than water and therefore might have a higher diffusion barrier, it might stay close to its original position. This conversion fits nicely with the fact that nothing remains after annealing water without having dosed $O_2$ before.

Dosing additional 0.015 L water with the sample at 290 K interestingly lead to appearance of water and OH (numbers in Table 3, image in Figure 21 **D**) instead of only OH, as it would be expected from the previous annealing. The appearance of water is surprising; a possible explanation is that the sample temperature was below the

intended temperature as the dosing process including warming up from 78 K took place within 4 minutes.

After annealing to 325 K (Figure 21 **E**), there was no significant change in $O_2$ coverage, while more water was converted into OH. This does not fit with the conversion of $H_2O$ and oxygen into OH. But possibly some oxygen is adsorbed at the step edges, which is reported to be stable at room temperature in [47] and could react with the additional water.

| What done | $H_2O$ coverage (%) | OH coverage (%) | $O_2$ coverage (%) | Image |
|---|---|---|---|---|
| Dose 0.015 L water | 3 | 0 | 0 | **A** |
| Dose $O_2$ | 3 | 0 | 0.8 | **B** |
| Anneal to 290 K | 0 | 1.1 | 0.2 | **C** |
| Dose 0.015 L water at 290 K | 0.7 | 0.6 | 0.1 | **D** |
| Anneal to 325 K | 0 | 1.3 | 0.1 | E |

**Table 3: Coverages of $H_2O$, OH and $O_2$ after consecutive treatment steps, image letters are from Figure 21**

If the abovementioned conversion of $H_2O$ and $O_2$ into OH does not happen, the H atom removed from the water needs to go somewhere. It might go into the bulk as it maybe happens with atomic hydrogen (see chapter 3.2.3) or it might desorb as $H_2$ when two water molecules come close enough to each other, converting both of them into OH.

The numbers in Table 3 are rather inaccurate, as the concentration of adsorbates varies over the position on the sample. This is most probably caused by varying defect and impurity concentrations. Additionally, not only reactions can happen, but adsorbates, especially $O_2$ and $H_2O$, might also simply desorb during annealing. As $O_2$ might as well adsorb at step edges, there might be some on the surface without being counted towards the coverage. All this makes it problematic drawing conclusions about the reaction mechanism from the number of adsorbates.

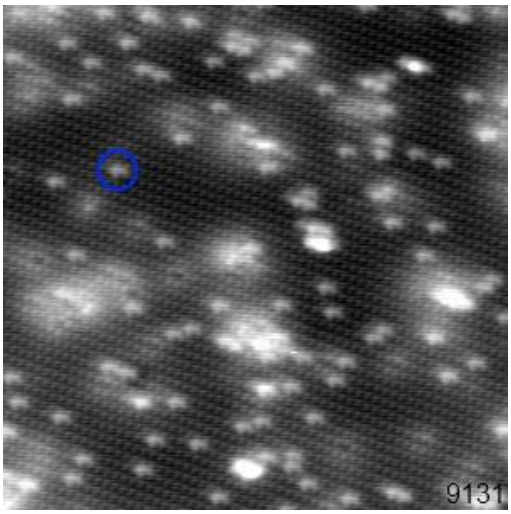


**A** 20×20 $nm^2$, 1 V, 0.09 nA

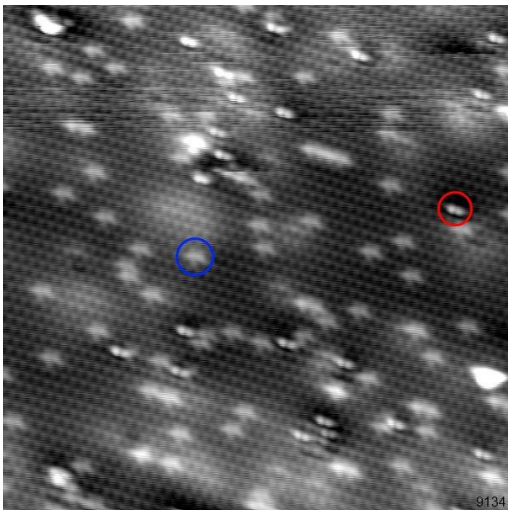


**B** 20×20 $nm^2$, 1 V, 0.09 nA

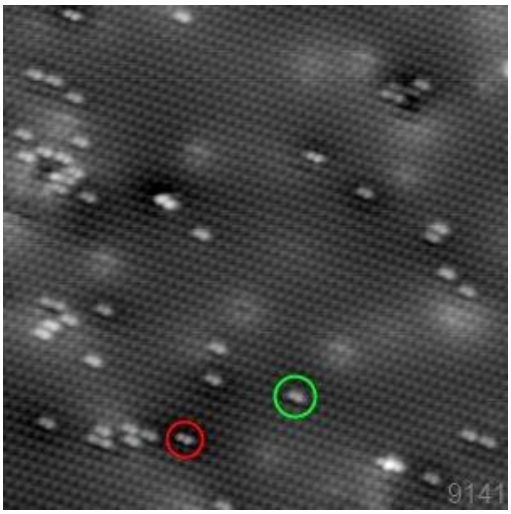


**C** 20×20 $nm^2$, 1 V, 0.09 nA

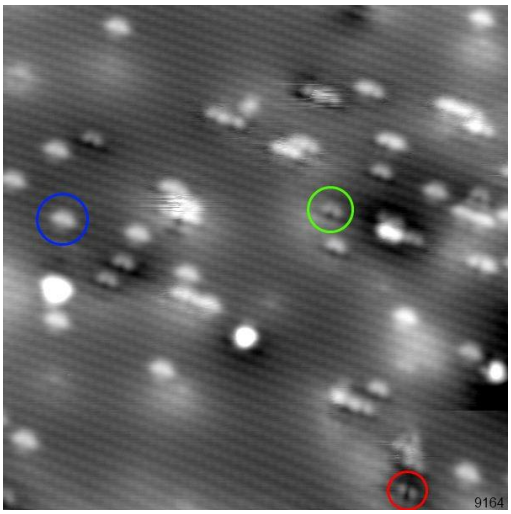


**D** 20×20 $nm^2$, 1 V, 0.09 nA

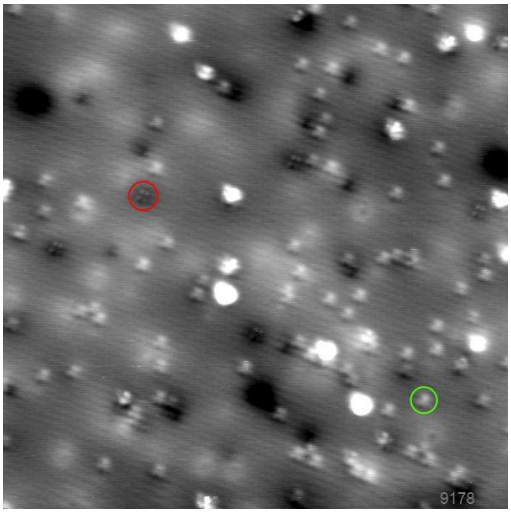


**E** 30×30 $nm^2$, 1.4 V, 0.08 nA

**Figure 21: Image series of the natural sample after subsequent treatments as listed in Table 3: dosing 0.015 L $H_2O$ at 130 K (A), 0.0375 L $O_2$ (B), annealing to 290 K (C), dosing additional 0.015 L $H_2O$ at 290 K (D), annealing to 325 K (E). Marked adsorbates: $H_2O$ (blue), $O_2$ (red), OH (green). After annealing to 290 K (C) water probably reacts with $O_2$ to OH, which shows an uneven distribution. After dosing additional water (D), both $H_2O$ and OH are found on the surface. Further annealing to 325 K (E) leads to more OH with no water left. The coverage of $O_2$ is unchanged after the last step.**

### 3.1.4 Summary

STM images of water are in agreement with simulated images and the calculated adsorption position with oxygen binding to $Ti_{5c}$ sites [41]. Usually $H_2O$ is dosed below 170 K; dosing at room temperature yields a clean surface. Between 250 and 290 K water desorbs from the surface, as is expected from TPD experiments [42]. However, with oxygen present on the sample, annealing desorbs only a part of the $H_2O$ and converts the rest into OH. The mechanism is not clear, but it might be 2 $H_2O$ molecules reacting with $O_2$ to form 4 OH. This idea provides an explanation for an uneven distribution of OH found after annealing, because it might be bound to the surface strong enough to be unable to diffuse far from the conversion site. Interactions of water with the STM tip were investigated; it is possible to convert $H_2O$ first into OH and then a bridging oxygen dimer. Tip-induced movement is observed rarely and usually in combination with conversion into OH or a bridging dimer.

## 3.2 Hydrogen

Molecular $H_2$ does not adsorb at all on most metal oxides, this was also calculated for the anatase (101) surface [48]. Dissociative adsorption was not observed, but might be slightly energetically favorable compared to a free $H_2$ molecule [48]. In this work atomic hydrogen was deposited on the surface with two different methods. One way is cracking $H_2$ gas at a hot tungsten filament close to the sample as described in chapter 2.5.3. The other way was by creating surface $V_O$s by electron irradiation (chapter 2.6) and dosing water. This way, the $H_2O$ molecule dissociates and its oxygen replaces the missing $O_{2c}$, leaving two neighboring H atoms on $O_{2c}$ sites behind as calculated in [49].

On rutile (110), hydrogen is already known from similar bridging OH groups that form after $H_2O$ dissociation at the usually present surface $V_O$s [20]. Atomic H was also dosed on rutile (110) at room temperature and found to have a saturation coverage of 70% [50].

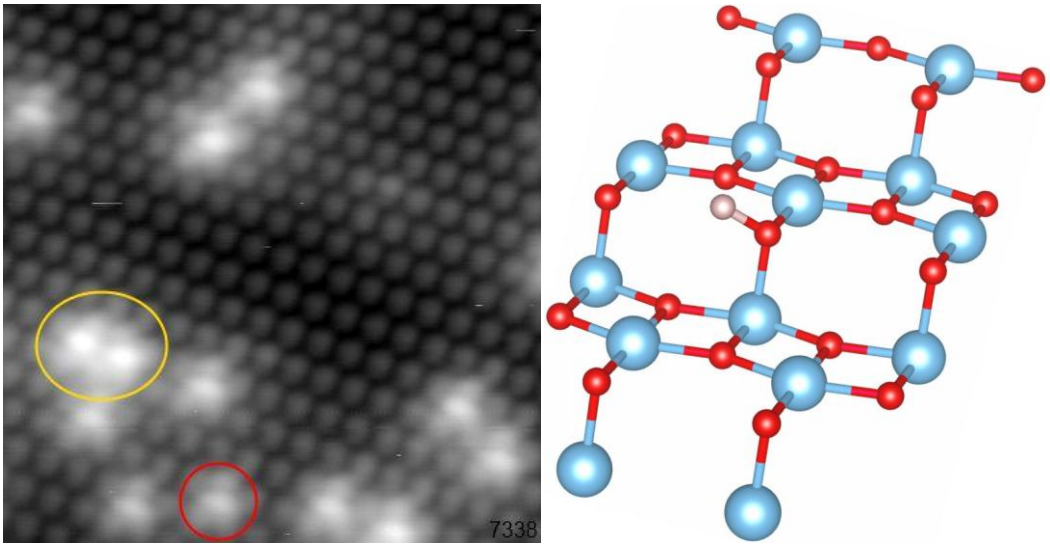


**Figure 22: Left: 6.6x6.6 nm$^2$, 0.8 V, 0.2 nA, high resolution STM image of hydrogen (2% coverage) adsorbed on anatase (101). Single H is marked red, two neighboring H (yellow) show an asymmetric appearance. Right: ball-and-stick model of the anatase (101) surface layer with adsorption position of H according to ref. [48].**

Atomic hydrogen always adsorbs as a $H^+$ bound to a surface O atom, forming a bridging hydroxyl. The position is on one side of at an $O_{2c}$ site as displayed in Figure 22 (right), which is the energetically most favorable by 0.3 eV [48, 51]. The electron from the hydrogen atom is transferred to the empty Ti 3d states [51]. The elongated and symmetric appearance of H with respect to the $O_{2c}$ in STM images (Figure 22 left, marked red) could be caused by fast flipping of H between the two symmetric configurations. This is expected to have a low activation barrier of 0.05 eV [48]. But as the shape of H does not change when scanning at 6 K (Figure 23), where thermal activation of the $O_{2c}$ side switching is unlikely, one has to consider either interaction with the STM tip or flipping due to tunneling. It is also possible that not the H itself is imaged, but its influence on the nearest $O_{2c}$ and $Ti_{5c}$ atoms.

Two hydrogen atoms at neighboring $O_{2c}$ sites are slightly unfavorable by 0.05 eV [48] when compared to separate H, but some are nevertheless found on many images. They

differ from isolated H atoms by having an asymmetric appearance (Figure 22 left, marked yellow), indicating a tendency to stay point from each other. This is supported by molecular dynamics simulations in [48]. Sometimes even groups of three H atoms can be found, showing even stronger differences in appearance than 2 (Figure 24).

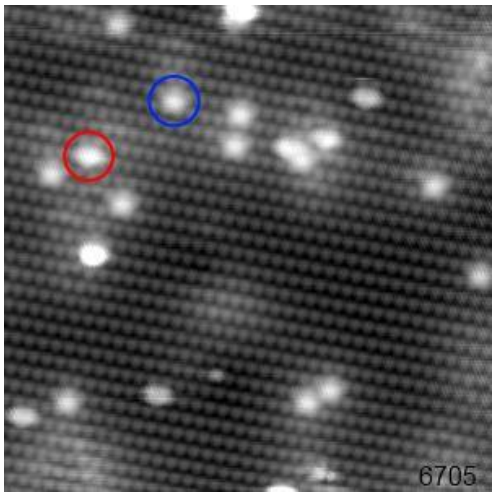


**Figure 23: 10x10 nm$^2$, 1 V, 0.5 nA, 6 K, 0.7% H (blue, 22.5 L dosed with the cracking filament), 0.3% $H_2O$ (red). When scanned at 6 K, hydrogen looks the same as when scanned at 78 K. No signs of H being fixed at one side of the $O_{2c}$ site were found.**

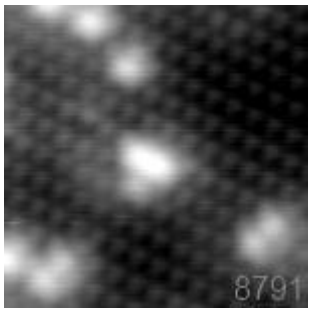


**Figure 24: 5x5 nm$^2$, 1 V, 0.1 nA, 5% H coverage. Sometimes even groups of 3 H atoms close together are found (in the center of the image).**

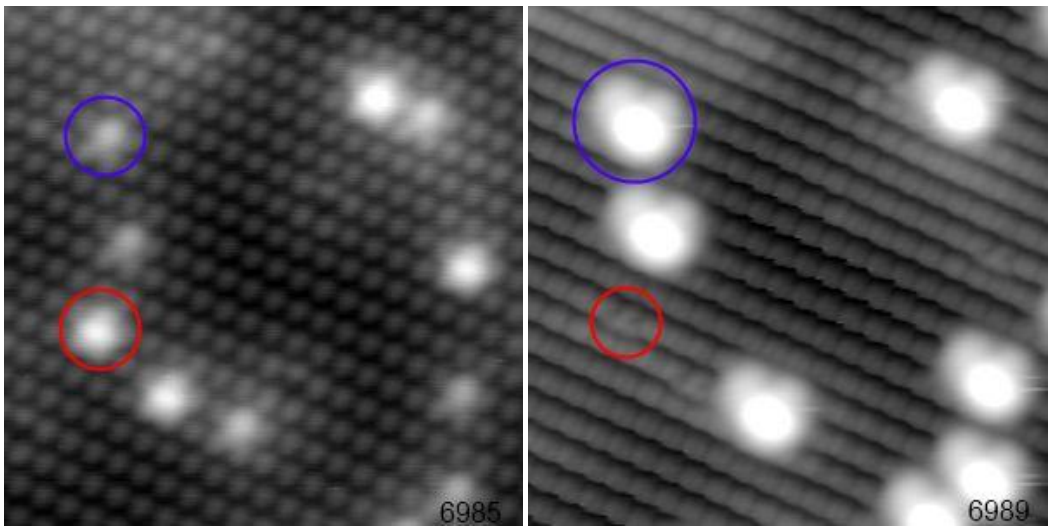


**Figure 25: 7.5x7.5 nm$^2$, 0.1 nA. All H comes from prior negative bias scan (see 3.2.2). The same area scanned with positive (1 V, left) and negative (-2 V, right) sample bias. H marked red, surface $V_O$s blue.**

When scanning at negative sample bias, hydrogen looks much less distinct than at the normally used positive bias voltage. In fact, it is very hard to spot without comparing it to an image of the same area taken at positive bias. In Figure 25 this comparison is made; there are also some surface $V_O$s visible that originate from scanning at high negative bias. Comparison of H with $V_O$s is also useful because they look somewhat similar. The clearest difference is the lower apparent height of $V_O$s. Furthermore, the bright spot from the $V_O$ is located at a $Ti_{5c}/O_{2c}$ site, while hydrogen has the bright spot between the rows.

### 3.2.1 Dosing hydrogen

#### *3.2.1.1 Direct dosing*

The direct dosing method with usage of a W cracking filament was described in chapter 2.5.3. The doses in Langmuir correspond to the amount of $H_2$ gas and are proportional to the amount of atomic hydrogen dosed on the sample. However, the given numbers of Langmuirs are only valid for the used setup. With a different filament and filament/sample distance some correction factor has to be determined to reproduce results from this work.

When dosing different amounts of hydrogen, the coverage was found to fit very well with an exponential approach towards a saturation coverage of 4.5-5% (Figure 26, STM image with 4.5% coverage in Figure 33 **A**. The formula for the least squares fit is $a\left(1-e^{-bd}\right)$ with the exposure d in Langmuirs and the fit parameters a=4.55624 and b=0.01256.

Initially H was dosed with the sample at temperatures from 100-130 K as it was not known until which temperature H would stay on the surface. Many of the later experiments, especially the ones with high hydrogen exposures, were done with the sample at room temperature. This prevents adsorption of residual water on the sample and makes scanning easier, as $H_2O$ coverages above 3% considerably reduce the image quality.

Interestingly, a trend of increasing H coverage for the same dosed amount was found for increasing temperatures from 125-270 K (Figure 27). No explanation for this behavior was found, but it might be related to the surface diffusion of hydrogen, which starts between 200 and 250 K.

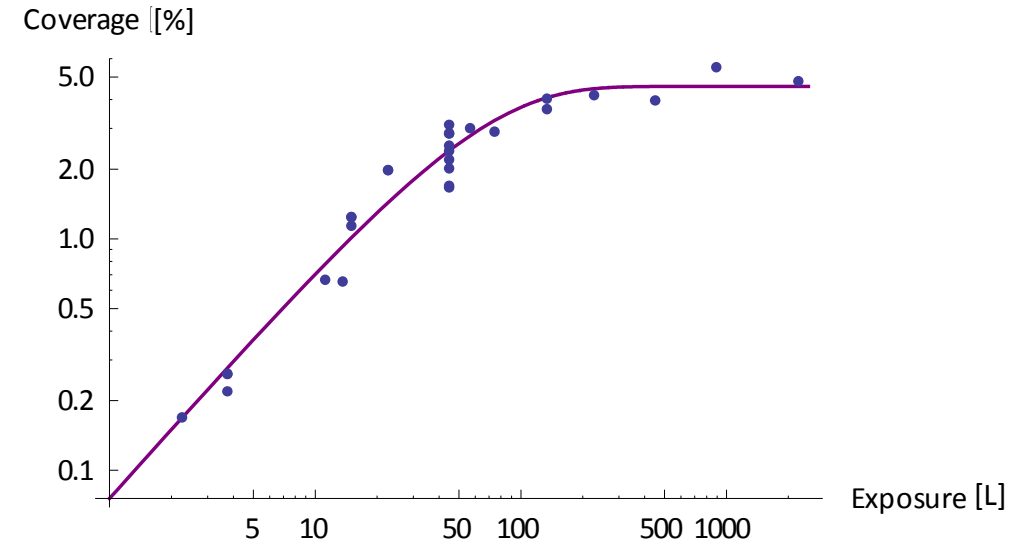


Figure 26: Hydrogen coverage versus exposure. Purple: A least squares fit for an exponential approach towards the saturation coverage. Exposures were done at different temperatures from 100 to 310 K.

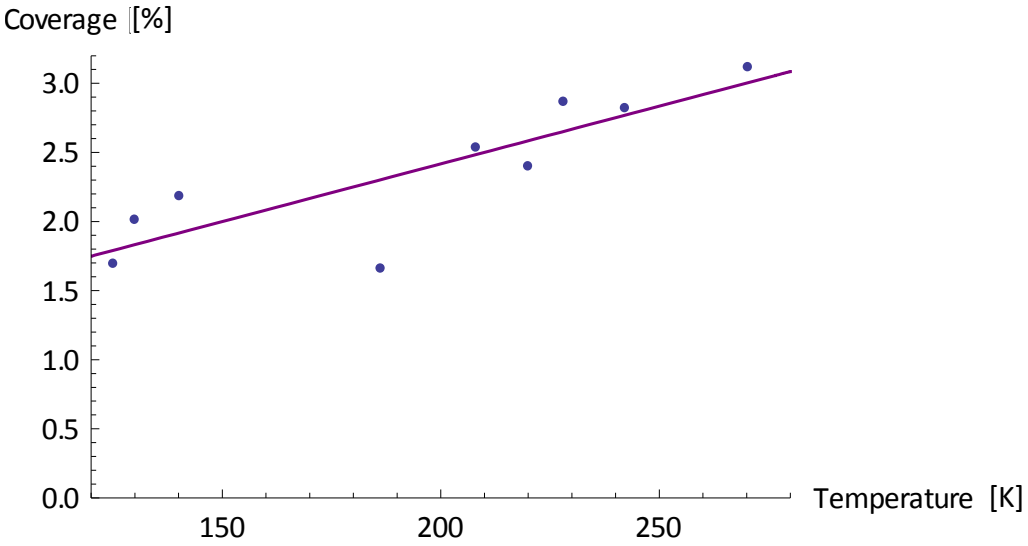


Figure 27: Hydrogen coverage varies for different sample temperatures after dosing 45 L, linear least squares fit in purple.

### 3.2.1.2 Dosing $H_2O$ on $V_O$s

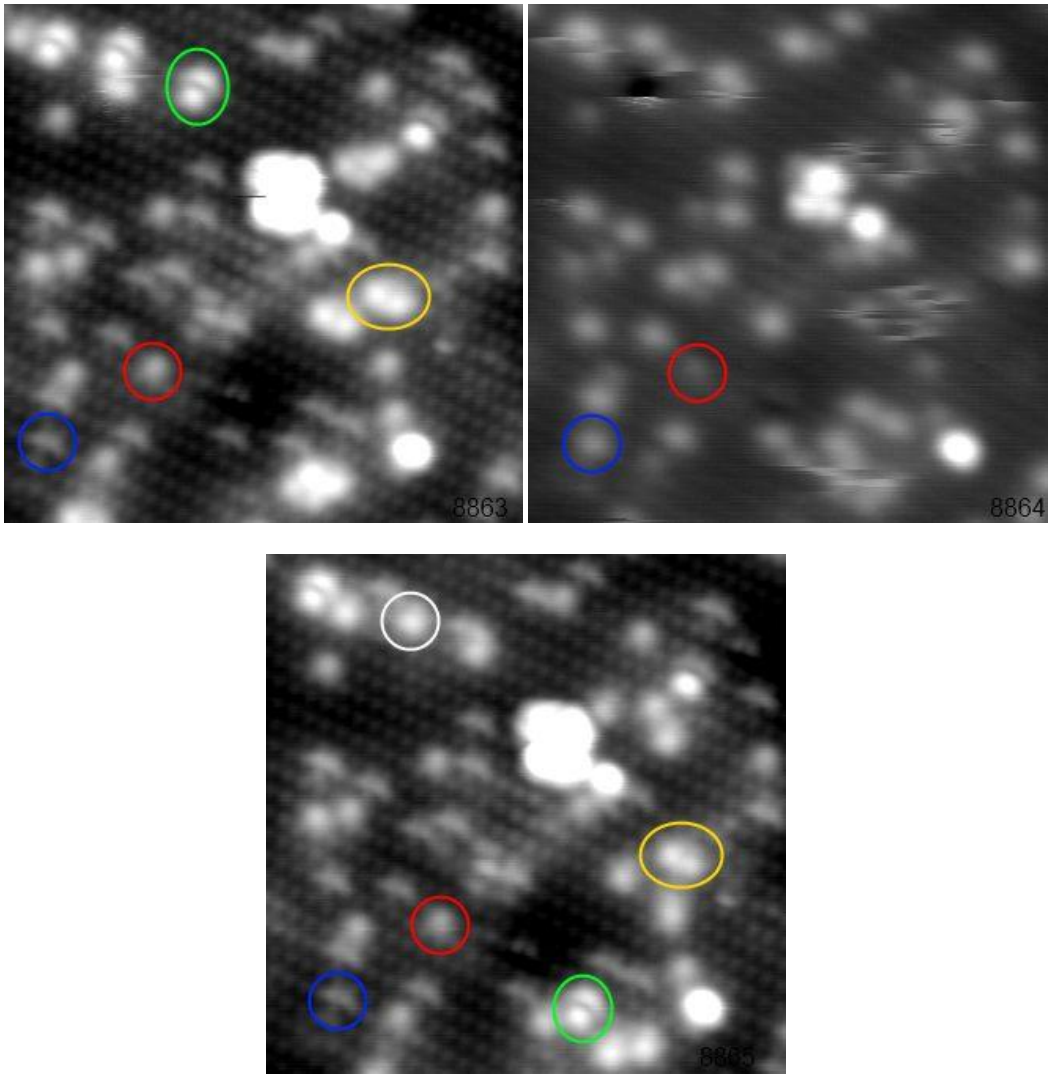


**Figure 28: 11x11 nm$^2$, 1 V, 0.1 nA, Anatase (101) after creating surface $V_O$s (red) and dosing 0.0075 L water (blue, 2% coverage) and annealing to 210 K. Initially hydrogen is found only in H pairs (yellow) and H/$H_2O$ pairs (green), after a 2.5 V scan (top right) also single H is found (white in the bottom image)**

H was also dosed indirectly by creating surface $V_O$s by electron bombardment (see chapter 2.6) and dosing water. At the typical dosing temperatures below 150 K the possibility of hitting a surface $V_O$ with a water molecule is rather low with a coverage of roughly 2% each. After annealing to temperatures around 210 K water starts diffusing on the surface and dissociates when it encounters a $V_O$, which results in two adjacent H atoms (Figure 28 top left, marked yellow). In this image not only pairs of adjacent H atoms can be seen, but also single H atoms in front of a water molecule (Figure 28, green). They can be identified by moving the H by scanning at a higher bias voltage (for more on tip induced movement see chapter 3.2.2). As these H/$H_2O$ pairs are the only other features than H pairs that contain atomic hydrogen, they probably originate from some kind of interaction of hydrogen with water. A good candidate is a mechanism similar to one that is known to occur on iron oxide [52]. In this publication, H-hopping was reported to happen via a $H_3O^+$ intermediate state. This water-driven H movement might also happen on anatase (101), as the used annealing temperature of 210 K is not high enough for H to diffuse on its own. The H/$H_2O$ features are probably what remains

from the $H_3O^+$ after cooling down. The water is assumed to stay because H makes the nearby $Ti_{5c}$ site more acidic, making it a preferred site for water adsorption.

Water was found to be stable immediately next to $V_O$s, even conversion to a bridging dimer by scanning at higher bias (see chapter 3.1.2) does not fill the adjacent $V_O$.

### 3.2.2 Interaction with the tip/behavior while scanning

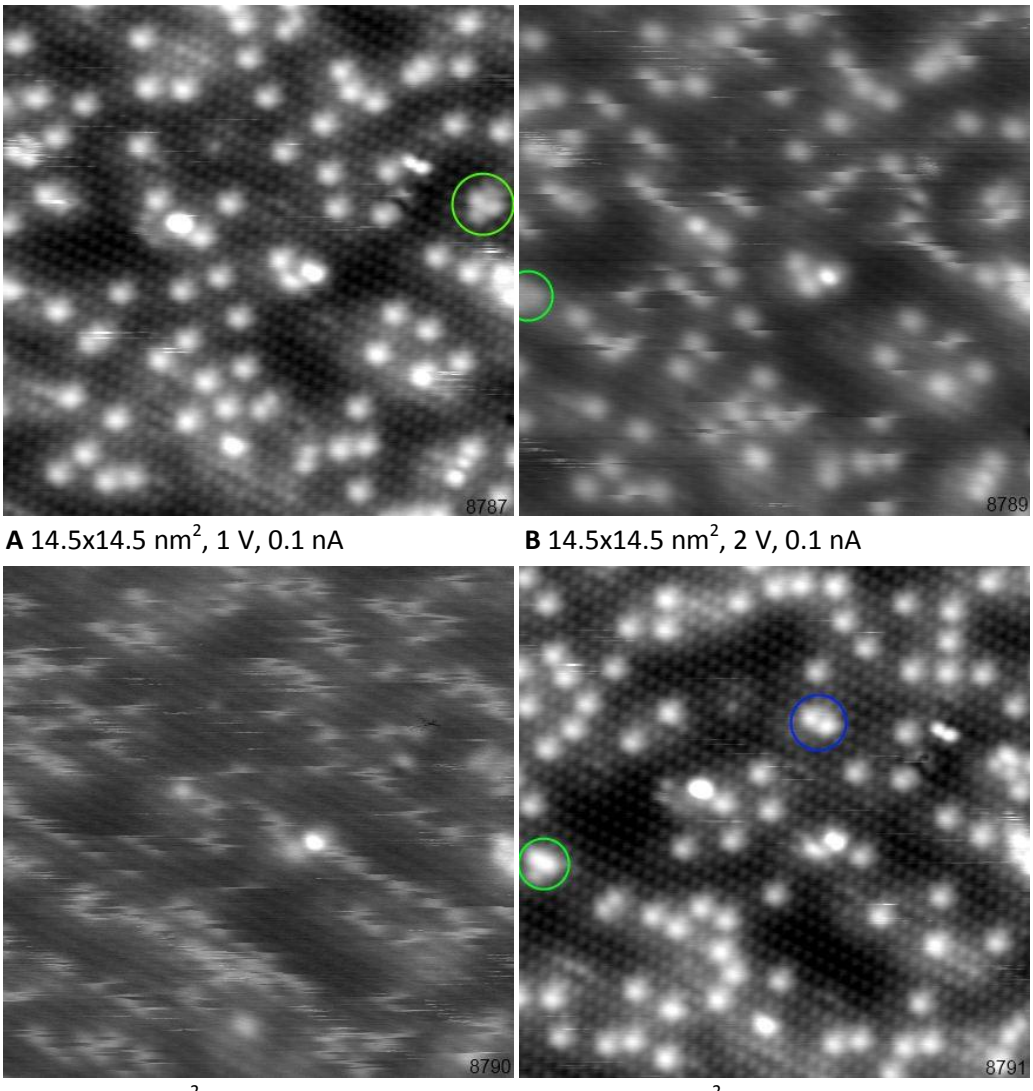


**A** 14.5x14.5 nm$^2$, 1 V, 0.1 nA

**B** 14.5x14.5 nm$^2$, 2 V, 0.1 nA

**C** 14.5x14.5 nm$^2$, 2.5 V, 0.1 nA

**D** 14.5x14.5 nm$^2$, 1 V, 0.1 nA

**Figure 29: Hydrogen covered surface (4.5% coverage) after creating surface $V_O$s, dosing 0.015 L $H_2O$ and annealing to 310 K. All images show the same area. Most of the hydrogen moves when scanning at 2 V (B), at 2.5 V (C) all H atoms are mobile. Groups of H atoms are marked blue (2 atoms) and green (3 atoms).**

The most noticeable interaction of H with the tip is the migration across the surface, which starts occurring when scanning with a bias above 1.5 V. With increasing bias, movement quickly gets stronger. While movement happens rarely at 1.5 V, and exclusively along the rows, at 2 V (Figure 29 **B**) roughly half of the H atoms move, with some rare jumps across the rows. Going higher, at 2.5 V (Figure 29 **C**) all H atoms move with very few exceptions, the direction along the rows remains dominant, although somewhat less than at 2 V. Scanning at 2.5 V and above also decreases the coverage, an

explanation of the related mechanism is given below**.** At 3 V movement happens very fast and H is barely visible in STM images, about 80% of the hydrogen is removed. Above 3.5 V no H is left in the scanned area (Figure 30).

Sometimes formations of 2 or 3 hydrogen atoms close together can be seen. For the pairs this was found to be unfavorable as mentioned above, but only slightly, so this can occur after moving H by high bias (Figure 29 **D**), marked blue). For 3 H atoms close together (Figure 29, marked green) there are no calculations, but they seem to be energetically roughly neutral as they have been observed several times. The observance that they can survive a 2.5 V scan, which was never seen with pairs, indicates that this configuration might be stabilized by the electric field of the tip or may be a bit more favorable than single atoms.

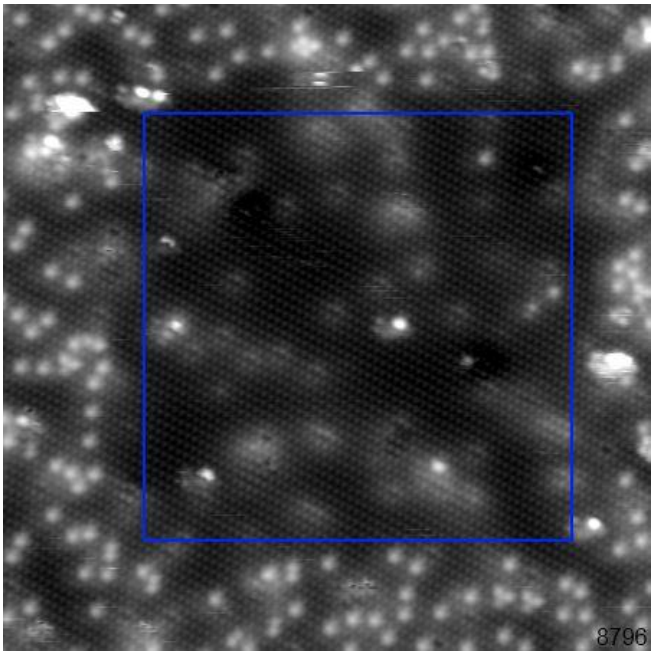


**Figure 30: 30x30 nm$^2$, 1 V, 0.1 nA, surface prepared as in Figure 29. H was removed by scanning the marked area with 3.5 V, the hydrogen was moved to the tip.**

The mentioned removal of H from the surface is likely to occur because of the negative bias of the tip relative to the sample. Since the adsorbed H is positively charged it is attracted by the tip. With a high enough bias the hydrogen is moved from the sample surface onto the tip. A good confirmation for this is that, when reversing bias below -2 V, hydrogen appears on the surface if the tip took up H before (Figure 31). The removal (and probably the reverse process too) is likely to be dependent on the electric field, which can be seen by the removal of hydrogen outside the area scanned at high bias (Figure 30).

Movement of H does not only happen when using positive sample bias, but sometimes also at negative bias below -2 V (Figure 32). This is probably influenced by tip changes as it does not always happen when scanning at negative bias. Movement does not increase when switching to lower negative bias.

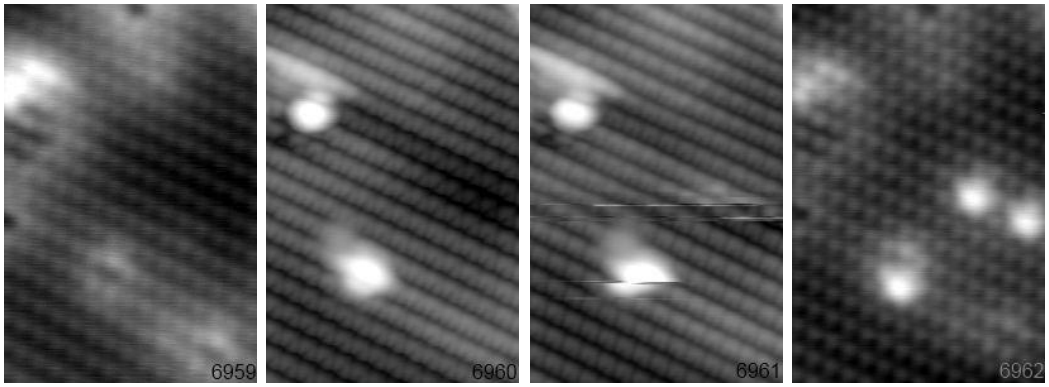


+1 V, 0.08 nA -1.5 V, 0.08 nA -2 V, 0.08 nA +1 V, 0.08 nA

**Figure 31: 5x7.5 nm$^2$, Consecutive scans of a clean surface, using a tip that was previously used to "clean off" H from the surface. Hydrogen appears on the surface while scanning at -2 V.**

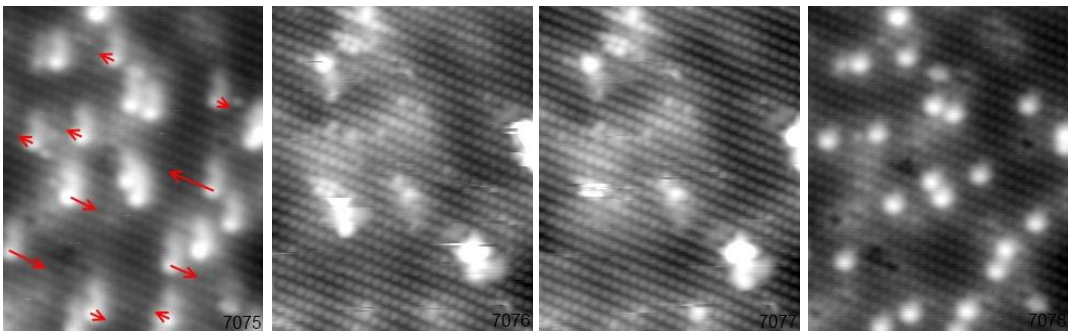


+1 V, 0.1 nA -2 V, 0.1 nA -2 V, 0.1 nA +1 V, 0.1 nA

**Figure 32: 10x12.5 nm$^2$, H (22.5 L $H_2$/hot filament, 2% coverage) dosed at 120 K. With some tips H is mobile while scanning at negative bias. The movement (direction and distance) is pointed out in the left image.**

### 3.2.3 Thermal stability

H does not diffuse at 210 K as can be seen from the sole occurrence of hydrogen as H-pairs and H/$H_2O$ pairs in Figure 28. Disappearance of almost all the H and H/$H_2O$ pairs after annealing to 260 K is a strong indication that at this temperature diffusion is already happening. From DFT calculations only diffusion along the rows is expected, as there is a calculated diffusion barrier of 0.6 eV, while across the rows the barrier is 1.82 eV [48]. The preference of movement along the rows is also seen in images with tip-induced movement in the previous chapter (3.2.2).

Hydrogen starts to disappear from the surface when annealing above 350 K, but with the methods used in the experiments it is not possible to decide whether it desorbs or it diffuses into the bulk. However, there are reasons that indicate that migration into the bulk is more likely. Calculations in [48] report a rather high barrier of 1.8-2 eV for recombinative desorption as $H_2$ and a considerably unfavorable (by 2.12 eV) desorption as $H_2O$ with creation of a surface $V_O$. A path for migration into the bulk, where adsorption is 0.4 eV less favorable than at the surface, with a lower barrier of 1.2 eV was predicted. Adsorption in subsurface $V_O$s was found to be energetically equivalent to a surface $O_{2c}$ site, but no migration paths into subsurface $V_O$s were calculated.

In two different experimental series partial disappearance of H above 350 K was found, but there were some seemingly contradicting results. With 2% H coverage, after annealing to 350 K for 10 min, 1.6% disappeared, leaving a coverage of 0.4%. In the second series, the coverage of initially 4.5% fell by 0.4% after annealing to 356 K for 5 min and then to another 1.9% after annealing to 374 K for 5 min; a coverage of 3.1% remained. This means that in the first series, 20% of the initial hydrogen were left, while in the second series 80% were left after annealing to the (almost) same temperature. A possible explanation is that 5 min might not be enough to stabilize the sample temperature, but even after annealing to 374 K 70% of the hydrogen stay on the sample. So another idea is that hydrogen migrates into some kind of rare and easily accessible site until all of these hypothetical sites are full, while the remaining H stays on the surface. Possible candidates for the sites are subsurface $V_O$s and Nb defect sites, but with the small number of experiments done, more are required to confirm this.

### 3.2.4 Potential subsurface H

When dosing with the filament, at very high H doses at the saturation coverage an increasing number of a certain defect type can be seen (Figure 33, red). Here, atomic H (2250 L $H_2$, $T_{sample}$ = 304 K) was dosed on the sample. For better visibility the surface hydrogen was removed by high bias scans in Figure 33 **B** and **D**. The 6 V scan before Figure 33 **D** allows comparison with the to some extent similarly looking surface $V_O$s and also shows the stability of the newfound defects where no change was observed. After annealing to 374 K (Figure 33 **C**) and **D** the number of the defects increased by roughly 50%.

While this kind of defect is sometimes also found with other surface preparations and at low H coverage, the low density of less than 1 in 10000 surface cells (corresponding to a 40x40 $nm^2$ image) makes a reliable identification hard. In the few experiments that were done with high H doses, the number of defects was found to increase in a linear fashion with the amount of H dosed (without annealing), indicating a clear correlation, see the right column in Table 4.

| Amount dosed (L) | Coverage (%) | Coverage per 10000 L (%) |
|---|---|---|
| 225 | 0.04 | 1.78 |
| 270 | 0.06 | 2.22 |
| 450 | 0.08 | 1.78 |
| 2250 | 0.4 | 1.78 |
| 2250 (annealed to 374 K) | 0.65 | 2.89 |
| 22.5 (annealed to 350 K) | 0.13 | 57.7 |

Table 4: Occurrence of the hydrogen related defects

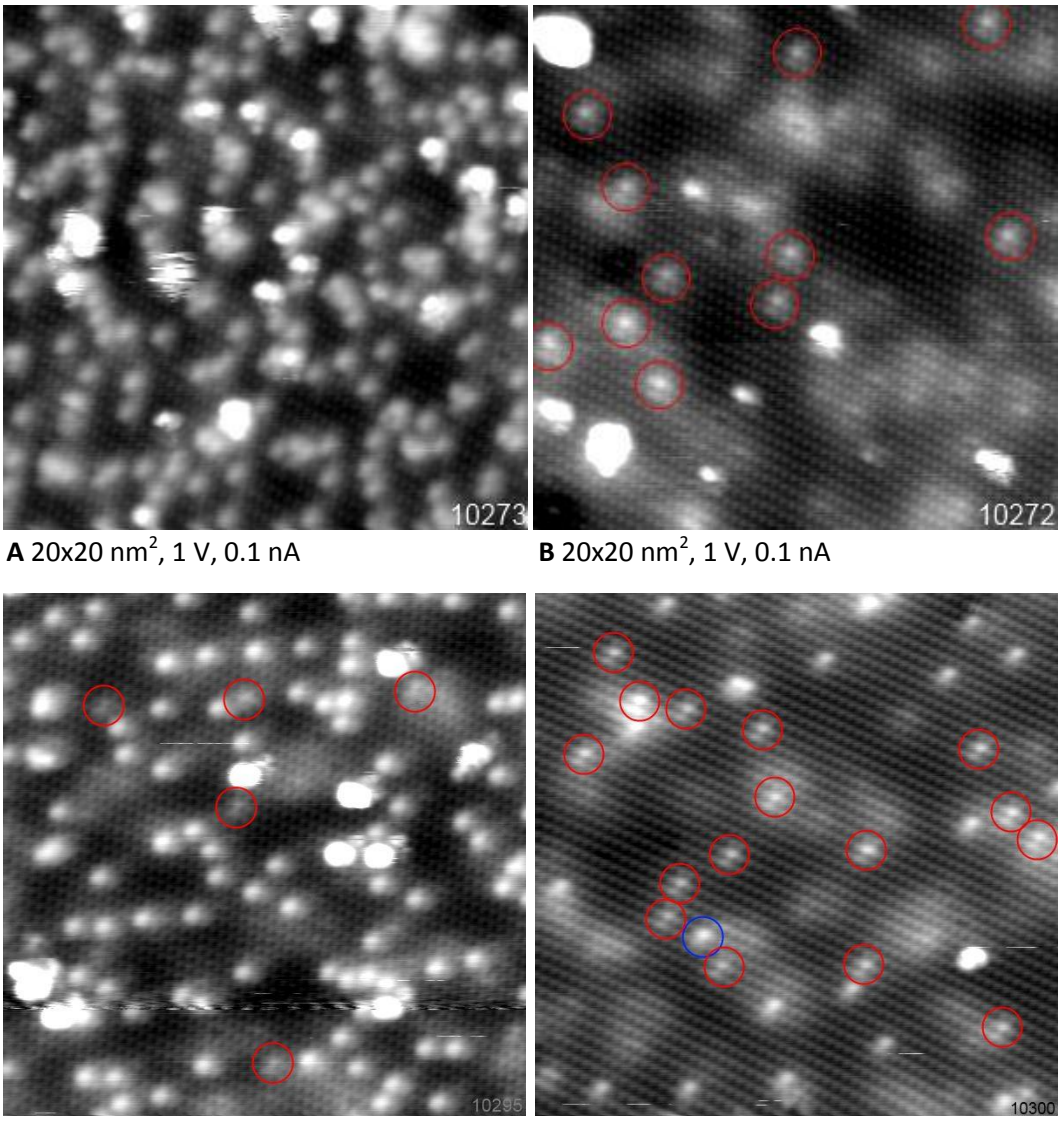


**A** 20x20 nm$^2$, 1 V, 0.1 nA **B** 20x20 nm$^2$, 1 V, 0.1 nA

**C** 20x20 nm$^2$, 1 V, 0.1 nA **D** 20x20 nm$^2$, 1 V, 0.1 nA

**Figure 33: The sample after H (2250 L $H_2$/hot filament, 4.5% coverage) dosing at 304 K (A, B) and subsequent annealing to 374 K (C, D). In B and D the hydrogen was removed by a 4 V (B) and a 6 V (D) scan, the latter one created surface $V_O$s (blue).**

While the reason for the defect is not known, the clear correlation with the amount of H dosed indicates that it is either some impurity coming from dosing or it is hydrogen adsorbed in an unlikely position. What speaks for a direct relation to H is that, after annealing to temperatures above 350 K, where H already disappears from the surface (see chapter 3.2.3), the number of these defects increases. The higher number of defects per 10000 L hydrogen dosed at the bottom of Table 4 (only 22.5 L dosed) hints that it might be an interaction of H with a rather rare type of surface or subsurface defect.

- One possibility is the Nb defect that is always present on the natural sample. While a rather low number of these Nb defects was found after dosing 2250 L hydrogen, it was still at the lower edge of the normally observed coverage of Nb defects, leaving much room for doubt.

- The second idea that the defect in question is a hydrogen atom attached to a subsurface O atom. According to DFT calculations in [48], this position is energetically unfavorable (compared to H on the surface) by 0.4 eV with a barrier for diffusion into the subsurface of 1.2 eV. While this diffusion might actually happen when annealing to 350 K, this idea does not explain the higher fraction of the defects after annealing 22.5 L when compared with 2250 L (in Table 4).
- In [48] the possibility of hydrogen adsorption in a subsurface $V_O$ is reported to be energetically equal to adsorption on a surface $O_{2c}$, but a diffusion barrier has not been calculated. The number of subsurface $V_O$s is not known as they are invisible under normal scanning conditions [2], but it is probably rather low.

### 3.2.5 Summary

Hydrogen was dosed in two ways: directly, using a hydrogen cracker, with a saturation coverage of 4.5-5% and by water dissociation on surface $V_O$s created by electron irradiation. The appearance of H in STM images fits with the calculated most favorable adsorption position at an $O_{2c}$ site [48]. Thermal stability was investigated; diffusion starts between 210 and 260 K, above 350 K hydrogen starts to disappear from the surface. The whereabouts of the removed H are not clear, but DFT calculations [48] and emergence of new subsurface defects after annealing indicate migration into the bulk. Interactions with the STM tip were investigated; H can be moved on the surface not only with positive bias between 1.5 and 3 V, but also, depending on the tip condition, with negative bias. At higher positive bias voltages H can be moved onto the tip, by switching to negative bias it can be moved back onto the sample.

## 3.3 $CO_2$

The $CO_2$ experiments were all done with liquid helium cooling at 6 K. There was one exception, where images were taken with the sample at 48 K, but this did not show any different results, thus the images are not included in this work. The low temperature was necessary because, while $CO_2$ should still be on the surface at 78 K according to the TPD spectra reported in [37], the molecules seem to be diffusing so fast that they cannot be imaged in STM except for a noticeable increase in noise. It is also likely that there is a more favorable adsorption position, maybe at step edges, because after dosing at 78 K and cooling to 6 K, no $CO_2$ is found. Most of the work on $CO_2$ was done on the synthetic sample.

According to ref. [38] $CO_2$ adsorbs at a $Ti_{5c}$ site as shown in Figure 34 with the most favorable position on the left. STM images (Figure 35) agree with these DFT calculations and often show a specific curved shape that may be attributed to rotation of the molecule, which does not cost much energy (0.06 eV at 90 degrees), while under the tip. On STM images of $CO_2$ on rutile (110), this rotation was found to determine the appearance of $CO_2$ [53], which is also located in a tilted position on a $Ti_{5c}$ [54].

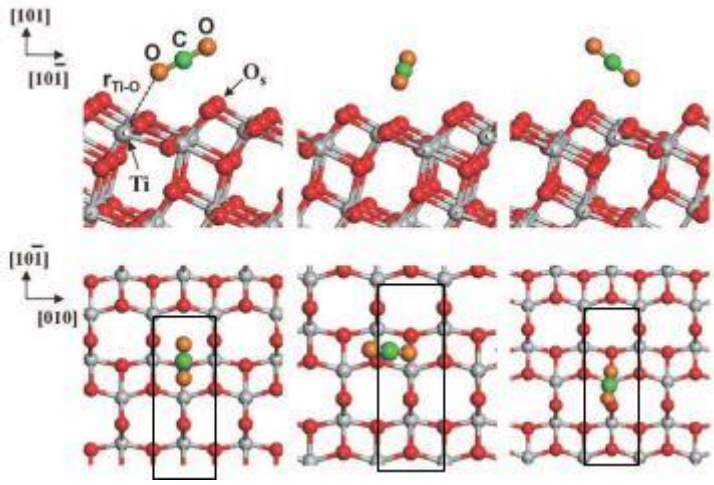


**Figure 34: Possible $CO_2$ adsorption positions (binding energies: 0.48, 0.42 and 0.34 eV from left to right) from [38]. The unit cell is marked as seen in Figure 35. $CO_2$ can adsorb to any of the equivalent $Ti_{5c}$ atoms at the corners or in the center.**

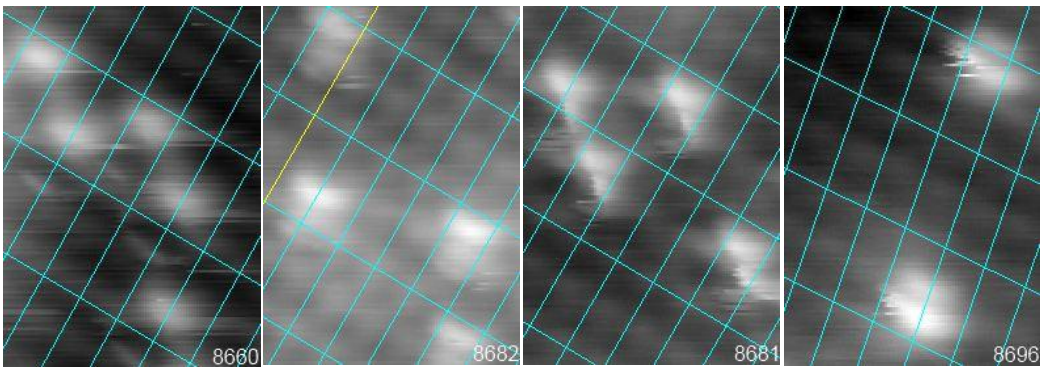


**Figure 35: 1.5×2.3 $nm^2$, 1 V, 0.07 nA, 0.0375 L (first 3 images) and 0.0075 L (right image) $CO_2$ dosed on the natural sample; anatase unit cell overlaid. $CO_2$ adsorbs at $Ti_{5c}$ sites at the grid corners and in the unit cell center. While there are many tip changes with $CO_2$, it is usually seen with a slightly curved shape when scanned at 1 V.**

Similar to hydrogen, the behavior of $CO_2$ shows a strong dependence on the bias voltage. While movement does not become as fast and frequent as it does with H, the $CO_2$ movement also mainly happens along the rows, which is in agreement with calculations in [38], where a lower activation energy of 0.19 eV along the rows and a higher one of 0.36 eV across the rows is mentioned. Desorption starts happening at 2 V, but is not very common. At 4 V all of the $CO_2$ desorbs (Figure 36 **C**). Most likely the molecule desorbs intact as there are no remains such as O or CO left on the surface.

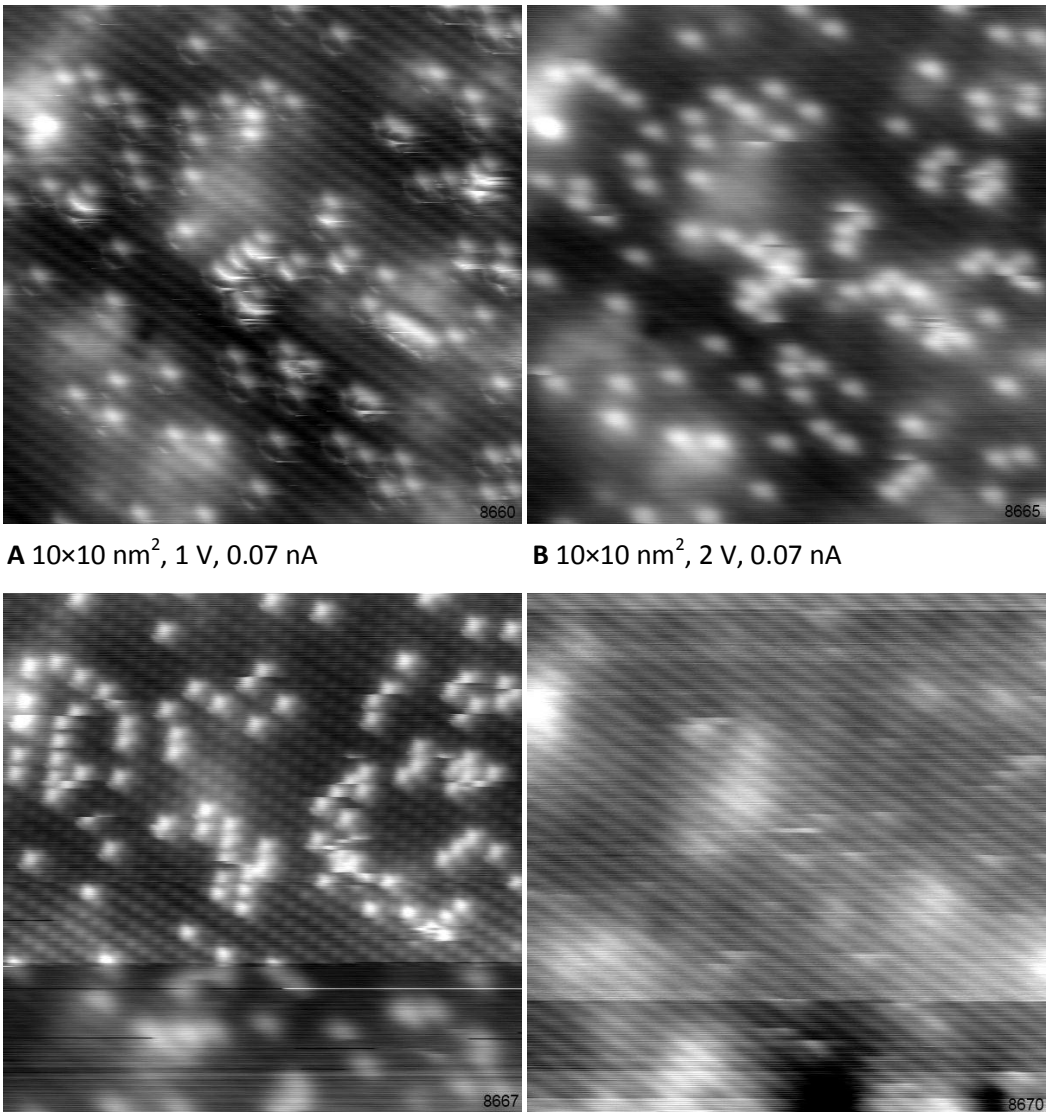


**A** 10×10 nm$^2$, 1 V, 0.07 nA

**B** 10×10 nm$^2$, 2 V, 0.07 nA

**C** 10×10 nm$^2$, 3 V, 0.07 nA

**D** 10×10 nm$^2$, 4 V, 0.07 nA

**Figure 36: 0.0375 L $CO_2$ dosed on the natural sample, all scans show the same area. After several scans at 1.5 V, clusters are seen in B. At 3 V (C) lines are found that originate from movement of $CO_2$ by the tip. At 4 V all $CO_2$ desorbs (D).**

In cases where the tip-induced movement is strong enough, formation of clusters (Figure 36 **B** and **C**, Figure 38 **B**) and lines (Figure 36 **C** and Figure 37, marked red) can be seen, although in some cases the lines seem to be caused by few molecules jumping across the rows towards the tip rather than actual lining up of several molecules. An example of this apparent line formation is given in Figure 36, where the number of molecules decreases from initially 88 (**A**) to 81 (**B**) over the course of several scans at 1.5 V and then seemingly jumps up to 110 during a 3 V scan (**C**). Most of these “additional”

molecules are located in lines, indicating movement towards the tip in the slow scan direction (from bottom to top). Movement along and across the rows occurs rarely at low bias and increases in frequency and moved distance when going up to 3 V.

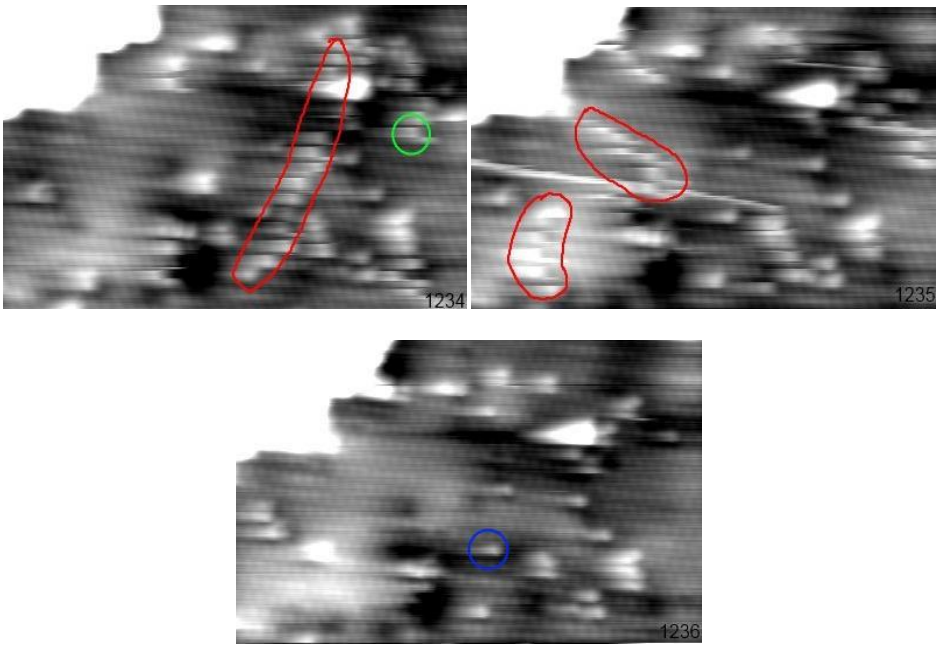


**Figure 37: 10×6.5 nm$^2$, 1.8 V, 0.13 nA, 0.15 L $CO_2$ dosed on the synthetic sample. $CO_2$ (green) sometimes shows high mobility on the synthetic sample. The tendency to form lines (red) indicates interaction between the molecules. $CO_2$ moves out of the scanned area over the course of 2 consecutive scans. The immobile spots (blue) are Ta as mentioned in chapter 2.3.2.**

In contrast to the apparent lines in Figure 36 **C**, the one in the top images Figure 37 (on the synthetic sample, marked red) is presumably real as it is seen in two consecutive images and thus cannot be a single molecule following the tip. Some form of interaction between $CO_2$ molecules might have lead to line formation, interaction is also indicated by the observation of clusters in Figure 36 and Figure 38. The rapid motion in Figure 37 at a bias of 1.8 V is unexpected, but high sensitivity of $CO_2$ mobility to tip changes is seen often, mostly on the synthetic sample. The reason why the synthetic sample behaves in a somewhat different way might be related to the less reduced state when compared to the natural one. This leads to a decreased conductivity and thus to a tip that comes closer to the surface, allowing for increased interaction with the adsorbates.

Formation of clusters is sometimes seen after scanning an area several times under tip conditions that allow the $CO_2$ to be moved (either via bias or “strange” tips that are often observed). In Figure 38 not only clustering, which happens while scanning the same area several times at 1 V, can be seen, but also removal of said cluster. This happens rather fast; after switching to 0.75 V bias, all of the $CO_2$ molecules leave the scanned area within 2 images. This indicates a stronger interaction with $CO_2$ when the tip is closer. In contrast to other cases of high mobility, the interaction with low bias was found to be independent of sample or tip changes.

A thing that can be seen in all images with strong $CO_2$ movement is that $CO_2$ seems to be located on top of the $Ti_{5c}/O_{2c}$ spots, while on the images with less movement/tip interaction the $CO_2$ molecules are visible at the position between the rows, as clearly

visible in Figure 35 and Figure 36. This is probably due to a stronger interaction even when the tip is rather far away. It seems that the molecules jump to the next easily available position away from the tip as soon as the tip comes somewhat close. This might be the reason why all the fast movements occur in the same direction (Figure 37 top and Figure 38 **C**) even though the tip is scanning forth and back.

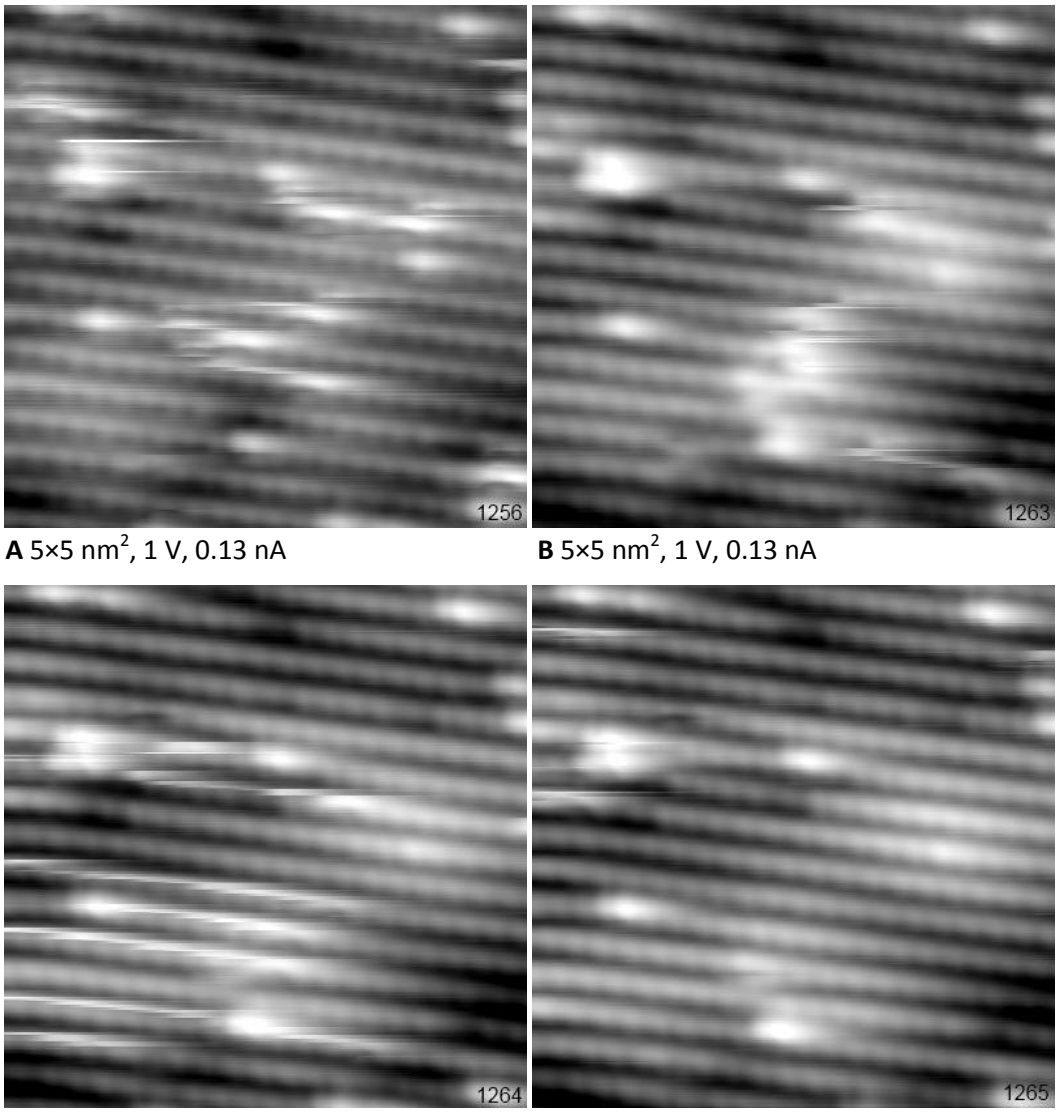


**A** 5×5 nm$^2$, 1 V, 0.13 nA

**B** 5×5 nm$^2$, 1 V, 0.13 nA

**C** 5×5 nm$^2$, 0.75 V, 0.13 nA

**D** 5×5 nm$^2$, 0.75 V, 0.13 nA

**Figure 38: 0.15 L $CO_2$ dosed on the synthetic sample, all scans show the same area. $CO_2$ clustering (B) occurs after several scans at 1 V. At 0.75 V (C) the tip is enough to remove almost all molecules from the scanned area (D).**

In summary, the adsorption position of $CO_2$ calculated in [38] fits with the STM images. $CO_2$ adsorbs with an oxygen atom to a $Ti_{5c}$ site, tilted towards neighboring $O_{2c}$ atoms. The shape in STM images is in good agreement with the energetically easy rotation of the molecule, similar to rutile [53]. $CO_2$ does not diffuse across the surface up to 48 K, while at 78 K it cannot be seen any more in STM. $CO_2$ was found to be moved by the tip both at high and low bias, with less movement in the range of 1-2 V. Interactions between the $CO_2$ molecules and with the STM tip were found. When scanning above 4 V $CO_2$ desorbs from the surface.

# 4 Summary

## *General introduction*

- The appearance of H, $H_2O$, OH and, to a somewhat lesser accuracy, $CO_2$ was determined.
- Adsorption positions of H, $H_2O$ and $CO_2$ were found to fit with prior DFT calculations; H binds to a surface $O_{2c}$ atom, while the other species bind with an oxygen atom to $Ti_{5c}$.

## *Atomic hydrogen*

- Atomic H was dosed from 100 K up to room temperature with a slight increase of the sticking probability with rising sample temperature.
- A saturation coverage of 4.5-5% was determined.
- Thermal removal of H starts at 350 K, but some hydrogen stays at the surface. This partial removal probably occurs by diffusion of H into subsurface $V_O$s, as indicated by an increasing occurrence of a certain type of subsurface defect.
- Hydrogen can be moved by the STM tip; at positive high bias it is picked up by the tip and can be transferred back onto the sample by switching to negative sample bias.
- Water can dissociate on (artificially created) surface $V_O$s, resulting in pairs of nieghboring H adatoms. Annealing above 210 K allows hydrogen to diffuse; this results in mostly single H atoms.

## *$H_2O$*

- Water was found to desorb between 250 and 290 K, in agreement with previous TPD experiments. In the presence of adsorbed oxygen, water is converted into OH when annealing.
- OH and water appear similar; likely OH adsorbs on $Ti_{5c}$ sites.
- The STM tip can convert water into OH and bridging oxygen dimers, lateral displacement was found to be a very rare occurrence.

## *$CO_2$*

- Adsorbed $CO_2$ molecules show strong interaction with the STM tip. The appearance in STM is governed by rotation of the molecule while scanning. Tip-induced movement is common at high and low bias with the latter being much more pronounced.
- Allowing $CO_2$ to move by scanning several times with appropriate settings leads to clustering, which indicates attraction between $CO_2$ molecules.
- $CO_2$ desorbs when scanned with high bias.

# 5 Bibliography


1. Diebold, U., *The surface science of titanium dioxide.* Surface Science Reports, 2003. **48**: p. 53-229.
2. Scheiber, P., *(Sub)Surface Mobility of Oxygen Vacancies at the $TiO_2$ Anatase (101) Surface.* Physical Review Letters, 2012. **109**: p. 136103.
3. Kamat, P., *Photochemistry on Nonreactive and Reactive (Semiconductor) Surfaces.* Chemical Reviews, 1993. **93**(1): p. 267-300.
4. Linsebigler, A., *Photocatalysis on $TiO_2$ Surfaces: Principles, Mechanisms, and Selected Results.* Chemical Reviews, 1995. **95**: p. 735-758.
5. Henderson, M., *A surface science perspective on $TiO_2$ photocatalysis.* Surface Science Reports, 2011. **66**: p. 185-297.
6. O'Regan, B., *A low-cost, high-efficiency solar cell based on dye-sensitized colloidal $TiO_2$ films.* Nature, 1991. **353**: p. 737–740.
7. Matsumura, M., *Dye Sensitization and Surface Structures of Semiconductor Electrodes.* Industrial & Engineering Chemistry Product Research and Development, 1980. **19**: p. 415-421.
8. Hamann, T., *Advancing beyond current generation dye-sensitized solar cells.* Energy & Environmental Science, 2008(1): p. 66-78.
9. Duonghong, D., *Dynamics of light-induced water cleavage in colloidal systems.* Journal of the American Chemical Society, 1981. **103**(16): p. 4685-4690.
10. Rajeshwar, K., *Hydrogen generation at irradiated oxide semiconductor–solution interfaces.* Journal of Applied Electrochemistry, 2007. **37**(7).
11. Nowotny, J., *$TiO_2$ Surface Active Sites for Water Splitting.* Journal of Physical Chemistry B, 2006. **110**: p. 18492-18495.
12. Dutta, P., *Interaction of Carbon Monoxide with Anatase Surfaces at High Temperatures: Optimization of a Carbon Monoxide Sensor.* Journal of Physical Chemistry B, 1999. **103**.
13. Lu, H., *Amorphous $TiO_2$ nanotube arrays for low-temperature oxygen sensors.* Nanotechnology, 2008. **19**.
14. Szot, K., *$TiO_2$—a prototypical memristive material.* Nanotechnology, 2011. **22**.
15. Yoon, I., *Memristor Behaviors of Highly Oriented Anatase $TiO_2$ Film Sandwiched between Top Pt and Bottom $SrRuO_3$ Electrodes.* Applied Physics Expess, 2011. **4**(041101).
16. Chopra, K., *Avalanche-Induced Negative Resistance in Thin Oxide Films.* Journal of Applied Physics, 1965. **36**(1).
17. Ohno, T., *Morphology of a $TiO_2$ Photocatalyst (Degussa, P-25) Consisting of Anatase and Rutile Crystalline Phases.* Journal of Catalysis, 2001. **203**: p. 82-86.
18. Lazzeri, M., *Structure and energetics of stoichiometric $TiO_2$ anatase surfaces.* Physical Review B, 2001. **63**.
19. Diebold, U., *One step towards bridging the materials gap: surface studies of $TiO_2$ anatase.* Catalysis Today, 2003. **85**(2-4): p. 93-100.
20. Schaub, R., *Oxygen Vacancies as Active Sites for Water Dissociation on Rutile TiO2 (110).* Physical Review Letters, 2001. **87**(26): p. 266104.
21. Hanaor, D., *Review of the anatase to rutile phase transformation.* Journal of Materials Science, 2011. **46**: p. 855-874.
22. Burdett, J., *Structural-electronic relationships in inorganic solids: powder neutron diffraction studies of the rutile and anatase polymorphs of titanium dioxide at 15*

*and 295 K.* Journal of the American Chemical Society, 1987. **109**(12): p. 3639-3656.
23. Schmid, M., *Experimentelle Methode der Oberflächenphysik, Lecture Notes*, 2011.
24. Kavan, L., *Electrochemical and Photoelectrochemical Investigation of Single-Crystal Anatase.* Journal of the American Chemical Society, 1996. **118**: p. 6716-6723.
25. Li, G., *Synthesizing mixed-phase $TiO_2$ nanocomposites using a hydrothermal method for photo-oxidation and photoreduction applications.* Journal of Catalysis, 2008. **253**: p. 105-110.
26. He, Y., *Evidence for the Predominance of Subsurface Defects on Reduced Anatase $TiO_2$ (101).* Physical Review Letters, 2009. **102**: p. 106105.
27. Cheng, H., *Surface and subsurface oxygen vacancies in anatase $TiO_2$ and differences with rutile.* Physical Review B, 2009. **79**(092101).
28. Ebert, P., *Nano-scale properties of defects in compound semiconductor surfaces* Surface Science Reports, 1999. **33**: p. 121-303.
29. Gong, X., *Steps on anatase $TiO_2$(101).* Nature Materials, 2006. **5**: p. 665-670.
30. Fidler, M., *STM Studie von Sauerstoffadsorption auf Defekten einer $TiO_2$ Anatas (101) Oberfläche*, 2011, Vienna University of Technology, Master Thesis.
31. Itaya, K., *Scanning tunneling microscope for electrochemistry - a new concept for the in situ scanning tunneling microscope in electrolyte solutions.* Surface Science, 1988. **201**(3): p. L507-L512.
32. Halbritter, J., *Tunneling mechanisms in electrochemical STM —distance and voltage tunneling spectroscopy.* Electrochimica Acta, 1995. **40**(10): p. 1385-1394.
33. Sueur, H.l., *Cryogenic AFM-STM for mesoscopic physics*, 2008.
34. Cricenti, A., *Preparation and characterization of tungsten tips for scanning tunneling microscopy.* Review of Scientific Instruments, 1994. **65**(5).
35. Binning, G., *Surface Studies by Scanning Tunneling Microscopy.* Physical Review Letters, 1982. **49**(1): p. 57-61.
36. Setvin, M., *Reaction of $O_2$ with Subsurface Oxygen Vacancies on $TiO_2$ Anatase (101).* Science, 2013. **341**: p. 988-991.
37. Suriye, K., *Control of $Ti^{3+}$ surface defect on $TiO_2$ nanocrystal using various calcination atmospheres as the first step for surface defect creation and its application in photocatalysis.* Applied Surface Science, 2006. **253**: p. 3849-3855.
38. Sorescu, D., *$CO_2$ adsorption on $TiO_2$ (101) anatase: A dispersion-corrected density functional theory study.* Journal of Chemical Physics, 2011. **135**.
39. Hickmott, T., *Interaction of Hydrogen with Tungsten.* Journal of Chemical Physics, 1960. **32**: p. 810-823.
40. Knotek, M., *Ion Desorption by Core-Hole Auger Decay.* Physical Review Letters, 1978. **40**(14).
41. He, Y., *Local ordering and electronic signatures of submonolayer water on anatase $TiO_2$ (101).* Nature Materials, 2009. **8**.
42. Herman, G.S., *Experimental Investigation of the Interaction of Water and Methanol with Anatase - $TiO_2$ (101).* Journal of Physical Chemistry B, 2003. **107**: p. 2788-2795.
43. Tilocca, A., *Reaction pathway and free energy barrier for defect-induced water dissociation on the (101) surface of $TiO_2$ -anatase.* Journal of Chemical Physics, 2003. **119**(14).
44. Lee, J., *Water Chain Formation on $TiO_2$ (110).* Journal of Physical Chemistry Letters, 2013. **4**: p. 53-57.

45. Aschauer, U., *Influence of Subsurface Defects on the Surface Reactivity of $TiO_2$: Water on Anatase (101).* Journal of Physical Chemistry C, 2010. **114**: p. 1278-1284.
46. Walle, L., *Mixed Dissociative and Molecular Water Adsorption on Anatase $TiO_2$ (101).* Journal of Physical Chemistry C, 2011. **115**: p. 9545-9550.
47. Setvin, M., *Charge Trapping at the Step Edges of $TiO_2$ Anatase (101).* Angewandte Chemie, 2014. **53**(18): p. 4714–4716.
48. Aschauer, U., *Hydrogen interaction with the anatase $TiO_2$ (101) surface.* Physical Chemistry Chemical Physics, 2012. **14**: p. 16595-16602.
49. Tilocca, A., *Structure and Reactivity of Water Layers on Defect-Free and Defective Anatase $TiO_2$ (101) Surfaces.* Journal of Physical Chemistry B, 2004. **108**: p. 4743-4751.
50. Yin, X., *Diffusion versus Desorption: Complex Behavior of H Atoms on an Oxide Surface.* ChemPhysChem, 2007. **9**: p. 253-256.
51. Islam, M., *Hydrogen Adsorption and Diffusion on the Anatase $TiO_2$ (101) Surface: A First-Principles Investigation.* Journal of Physical Chemistry C, 2011. **115**: p. 6809-6814.
52. Besenbacher, F., *Water-Mediated Proton Hopping on an Iron Oxide Surface.* Science, 2012. **336**: p. 889-893.
53. Lin, X., *Structure and Dynamics of $CO_2$ on Rutile $TiO_2$ (110)-1×1.* Journal of Physical Chemistry C, 2012. **116**(50): p. 26322–26334.
54. Sorescu, D., *$CO_2$ adsorption on $TiO_2$(110) rutile: Insight from dispersion-corrected density functional theory calculations and scanning tunneling microscopy experiments.* Journal of Chemical Physics, 2011. **134**(104707).